

Review

# An Overview of Electrochemical Energy Storage Devices of Various Electrodes and Morphological Studies of Supercapacitors

R. Ramachandran<sup>1</sup>, Shen-Ming Chen<sup>2,\*</sup>, G. Gnana kumar<sup>3</sup>

<sup>1</sup>Department of Chemistry, The Madura College, Vidya Nagar, Madurai – 625 011, Tamil Nadu, India.

<sup>2</sup>Electroanalysis and Bioelectrochemistry Lab, Department of Chemical Engineering and Biotechnology, National Taipei University of Technology, No.1, Section 3, Chung-Hsiao East Road, Taipei 106.Taiwan (ROC)

<sup>3</sup>Department of Physical Chemistry, School of Chemistry, Madurai Kamaraj University, Madurai-625 021,Tamil Nadu, India.

\*E-mail: [smchen78@ms15.hinet.net](mailto:smchen78@ms15.hinet.net)

Received: 6 August 2015 / Accepted: 9 September 2015 / Published: 4 November 2015

---

A novel based electrochemically active various electrodes (Carbon nanotube, metal oxides, conducting polymers and nanocomposites) materials has been overviewed for the development of supercapacitor applications. Different kinds of morphological (Flowers, nano fibers, nano wires, nano rod and nanoporous) based electrodes were reported reasonable specific capacitance, specific power, specific energy and excellent cyclic stability etc. The necessity of energy storage devices extremely focused on the following parameters such as cost-effective, cycle life and safety usage. In spite of that, the need of supercapacitors achievements in higher specific capacitance and long-durability of the electrochemical reaction have been carried out. In this article, we studied the different choice of electrode materials, capacitors classifications, morphological structure, BET surface and electrochemical optimization of the overall supercapacitors performance. Recently, most of the researchers have significantly addressed nanocomposite electrodes, because of, due to increase the BET surface area, narrow sized distribution and improve their supercapacitors (Specific capacitance, specific powers, specific energy and cyclic durability) parameters. The above discussed over all surveys literatures of electrochemical parameters, which can be used as emerging technologies for supercapacitors.

---

**Keywords:** Electrode materials, Nanocomposites, Specific capacitance, Supercapacitors, Morphological studies, Electrochemical analysis.

## 1. INTRODUCTION

The main focused on supercapacitor studies, which can be used at various electrode materials for the productions of electrical energies and power densities. Supercapacitors are considered as a

green energy source and it can be mainly applied with various fabrication/synthesis methods. It is one of the best primarily available source in green energy technology [1, 2]. The high surface area ( $1344 \text{ m}^2 \text{ g}^{-1}$ ) and large pore volume ( $0.902 \text{ cm}^3 \text{ g}^{-1}$ ) of nitrogen-doped mesoporous/microporous carbon (NMMC) based electrode used in supercapacitor, which has the delivered capacitance value of  $325 \text{ F g}^{-1}$  [3]. Zhang *et al* [4] used hydrothermal-assisted one step solution phase method for the synthesis of RGO/ $\text{Ni}_3\text{S}_2$  on nickel foam electrode, the superior performed capacitance value of  $2188.8 \text{ F g}^{-1}$  at  $2.9 \text{ A g}^{-1}$ . In 2014, Xing *et al* [5], reported a method of synthesis through the hydrothermal template route of  $\text{CoS}_2$  octahedrons in pseudocapacitive ( $236.5 \text{ F g}^{-1}$ ) applications and the remarkable retention stability up to 2000 cycles. In order to prepare a hollow melamine resin-based carbon spheres/graphene composite by polycondensation method. Here, polyvinyl alcohol play an important role to control their structure and size, the 3D-network composite achieved their excellent specific capacitance value of  $720 \text{ F g}^{-1}$  [6]. The most widely used graphene (Graphene nanosheets/porous carbon) based composite, the observed specific capacitance value of  $410 \text{ F g}^{-1}$  in  $6\text{M KOH}$  [7]. Chen *et al* [8], fabricated a 3D choleat-like polypyrrole  $\text{Ni@MnO}_2\text{@PPy}$  composite, showed their improved specific capacitance value of  $191.3 \text{ F g}^{-1}$  in  $0.5\text{M Na}_2\text{SO}_4$  aqueous solution. Surface activated carbon aerogel (ACA) has been extensively used in supercapacitor studies, from the cyclic voltammetry measurement, the estimated specific capacitance value around  $140 \text{ F g}^{-1}$  [9]. Aluminium-substituted  $\alpha$ -cobalt hydroxide has been already exhibited a wealth of structure and surface morphology. The versatile, unique electrode properties were obtained the high-tech energy ( $843 \text{ F g}^{-1}$ ) storage devices [10]. Carbon nanotube supported nickel hydroxide ( $\text{Ni(OH)}_2/\text{CNT}$ ) composite is considerable to be a promising electrode materials for the production of high specific capacitance and maximum specific power respectively [11]. A low-cost and high performance L-Cysteine supported  $\text{CoS}$  nano spheres and nanowires have been synthesized by hydrothermal method, the remarkable obtained capacitance value of  $508 \text{ F g}^{-1}$  [12]. Guo and Gao [13] delivered boron and nitrogen-doped porous carbon (BNC) electrode prepared in a facile pyrolysis route provided a large specific capacitance value of  $268 \text{ F g}^{-1}$ . Hwang *et al* [14] synthesized a kind of high specific surface area ( $300\text{-}400 \text{ m}^2 \text{ g}^{-1}$ ) nanoporous carbon aerogels via RF wet gel method. The special porous network structures lead their fine capacitance ( $220.4 \text{ F g}^{-1}$ ) value. In the previously reported category of poly(3,4-ethylenedioxy thiophene)/polypyrrole (PEDOT/PPy) composite has been focused as a new tendency in the evaluation of their structural (Horn-like structure), electrochemical and cyclic stabilities [15]. Kim *et al* [16] has extensively studied electrochemical properties of Ru-Co mixed SWCNT composite, because they were used as a active electrode materials in high performance ( $\sim 620 \text{ F g}^{-1}$ ) supercapacitor. The application of carbon nanofiber based poly(3,4-ethylenedioxythiophene)-poly(styrene sulfonate) composite to supercapacitors have been studied through galvanostatic charge-discharge method [17]. Carbon nanofibers (CNFs) have ladder-like structure, the diameter range from  $50\text{-}500 \text{ nm}$  and their increased specific surface area up to  $13\text{-}212 \text{ m}^2 \text{ g}^{-1}$ . The as-prepared ladder-like CNF could gained reasonable specific capacitance ( $\sim 60 \text{ F g}^{-1}$ ), specific power ( $\sim 100\text{W kg}^{-1}$ ) and its specific energy ( $1 \text{ Wh kg}^{-1}$ ) etc [18]., Supercapacitor based on manganese oxide based carbon ( $\text{MnO}_2/\text{C}$ ) composite has been synthesized by micro emulsion method. Such type of nano rod based  $\text{MnO}_2/\text{C}$  composite exhibited a good capacitive behaviour and the reported specific capacitance value of  $458 \text{ F g}^{-1}$  [19]. Nanoporous ruthenium oxide ( $\text{RuO}_2$ ) thin film has been prepared by a single step chemical method. The

nanoporous materials optical and absorption properties showed the direct band with the band gap value of 2.2 eV and the estimated capacitance value ( $50 \text{ F g}^{-1}$ ) in  $0.5\text{M H}_2\text{SO}_4$  at  $20 \text{ mV s}^{-1}$  [20]. The possible simple method was used for the preparation of activated carbon-semiconducting oxide ( $\text{TiO}_2$ ), the exhibited specific capacitance of over  $63.1 \text{ F g}^{-1}$  with high surface area of only  $1191 \text{ m}^2 \text{ g}^{-1}$  [21]. Now a day the most commercially available electrode materials have been used in various electrochemical applications such as sensors [22], pesticide sensors [23], solar cells [24], supercapacitors [26] and biosensors [26]. etc.

The aim of this article explained in the reported available literature at various electrode materials, different morphological structures, factors affecting parameters and various electrochemical techniques for the evaluation of supercapacitor performance. Most importantly, the authors have highlighted with the structures, morphologies, electronics, mechanical, thermal, specific power, specific energy and super capacitance properties etc. Finally, we concluded with the summary of the supercapacitors reported literatures, one of the major energy technologies could serve our future generations.

## 2. ELECTRODE MATERIALS

### 2.1. Carbon electrode

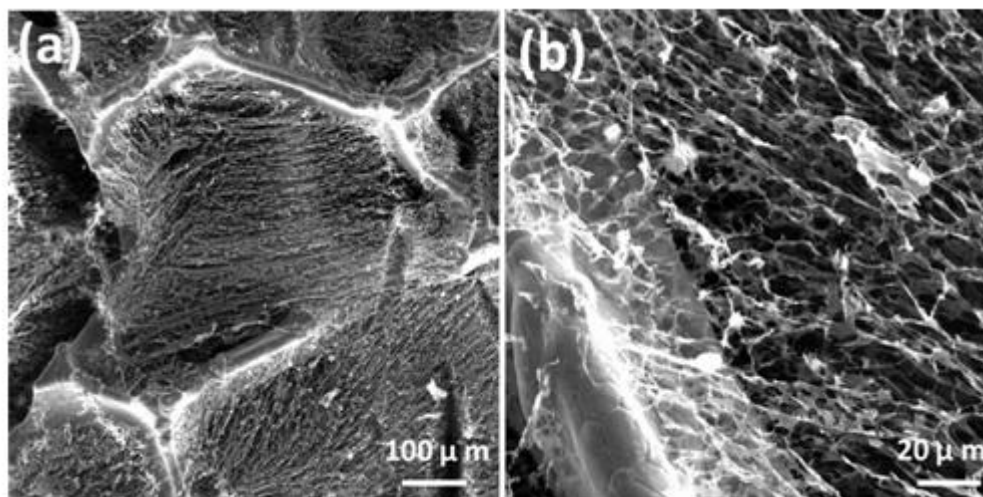


**Figure 1.** SEM images of as-prepared GCA@NF at different magnifications (a, b). ("Reprinted with permission from (*ACS. Appl. Mater. Interfaces*, 5 (2013) 7122). Copyright (2013) American Chemical Society").

A binder free of three-dimensional graphene aerogel has been deposited on nickel foam (GA@NF) by the facile two-step method. On the basis of the GA@NF electrode was exhibited their high rate capability, good electrochemical cyclic stability and specific capacitance value of  $366 \text{ F g}^{-1}$  at  $2 \text{ A g}^{-1}$  (Fig.1) [27]. The hierarchical reduced graphene based  $\text{MnO}_2$  (MnC/RGO) composite was fabricated through the electrostatic self-assembled method. The systematic electrochemical properties were investigated by charge-discharge, cyclic voltammetry and electrochemical impedance spectroscopy (EIS) methods, the achieved highest specific capacitance value of  $193 \text{ F g}^{-1}$  and the

retention (~70 %) cyclic stability for 1300 cycles [28]. The two-dimensional based  $\text{MnO}_2$  nanoplate, which can be modified with carbon nanotubes by sonication method. Here,  $\text{MnO}_2$  electrode exhibits poor electrical conductivity, by the addition of CNT nanotube, the electrode surface area increases with increased 8-order electrical conductivity evaluated by percolation theory [29]. The large surface area of ultrathin nitrogen-doped graphitic carbon nanocages electrode increases the electrochemical conductivity and desirable suitable performance ultra fast capacitance applications. The optimized (Annealed  $800^\circ\text{C}$ ) CNCs-800 electrode showed the specific capacitance value of  $248\text{ F g}^{-1}$  and an excellent electrical durability of 5000 cycles in 6M KOH [30]. Possibly, the template-free synthesis of macroporous carbon electrode has shown the sustainable development of next generation energy storage devices in high performance capacitor studies. In this electrode were clearly illustrated by the interpenetrating macroporous carbon based materials for the high performance ( $330\text{ F g}^{-1}$ ) capacitance behaviours evaluated by charge-discharge method [31]. Zhi *et al* [32] have used activated carbon for the extraction from waste tires by pyrolysis and chemical activation processes. The obtained electroactive carbon (WTAC) has been explored extensively for energy storage device applications and it was evaluated by both cyclic voltammetry and charge-discharge methods. In particular, the observed WTAC electrodes observed specific capacitance values were in good agreement with both the techniques (Cv and charge-discharge), WTAC-16 electrode reported the highest specific capacitance ( $106.4\text{ F g}^{-1}$ ) value than the others. Newly, designed and development of three-dimensional (3D) carbon nanotubes (CNTs) modified on highly porous carbon nanocups (CNCs) by anodization and chemical vapour deposition (CVD) techniques. The vertically aligned CNT-CNC hybrid composite has been developed by improving the possibility and finding of supercapacitor applications. The maximum obtained specific capacitance value of  $45\text{ F g}^{-1}$  and the cyclic stability tested up to 1000 cycles by charge-discharge method [33].

## 2.2. Metal oxides

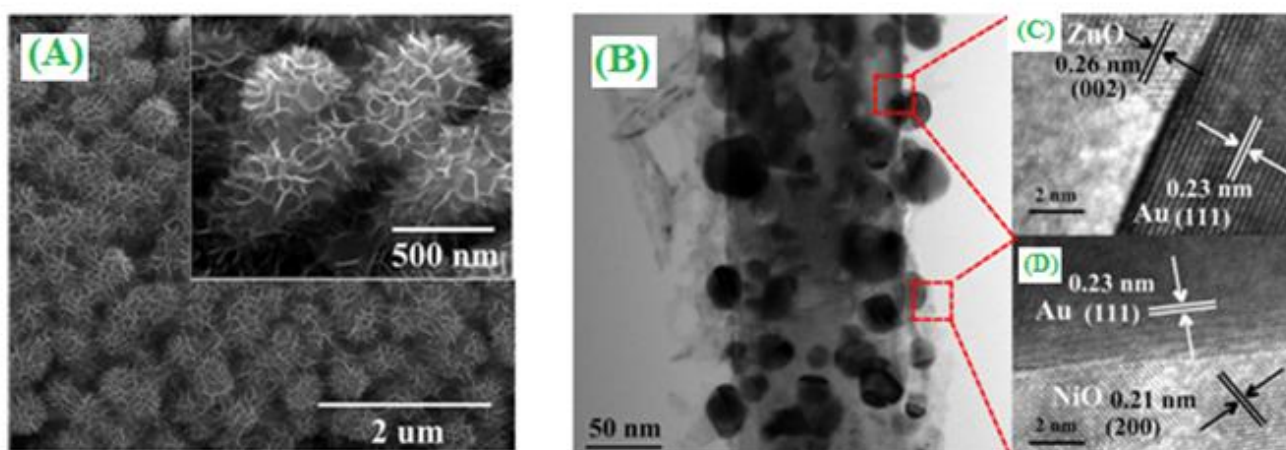
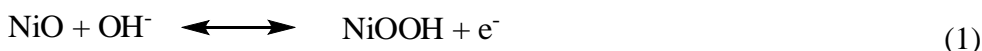


**Figure 2.** (A) SEM image of ZnO–Au–NiO hybrid composites (B) TEM images of ZnO@Au@NiO core–shell nanostructure and (C and D) the corresponding HRTEM images. ("Reprinted with permission from (*ACS. Appl. Mater. Interfaces*, 7 (2015) 2480). Copyright (2015) American Chemical Society").

The gold-supported ZnO/NiO core-shell composite was extensively evaluated for supercapacitor applications. The Au nanoparticles were implanted the strong interaction between ZnO nano rods and NiO nano sheets as shown in Fig.2, the Faradic electrochemical redox reaction, which was taking place as follows:



The core-shell based composite act as a promising electrode catalyst for the production of maximum capacitance ( $4.1 \text{ F cm}^{-2}$ ) behaviour at  $5 \text{ mA cm}^{-2}$  [34]. A 3D hierarchical flower-shaped nickel cobaltite ( $\text{NiCo}_2\text{O}_4$ ) microsphere electrode, which was synthesized by a rapid microwave-assisted method. The solution phase ( $R_s$ ) and charge-transfer ( $R_{CT}$ ) resistance has been estimated by Nyquist plot, the observed cyclic stability slightly increased their Warburg impedance during the 1000<sup>th</sup> cycles. Only 7 % electrode degradation was occurring and remarkably agreed with 1<sup>st</sup> cycle specific capacitance ( $1006 \text{ F g}^{-1}$ ) result [35]. A novel, environmentally friendly and scaffold mesoporous CoO nanocubes@ continuous 3D carbon based electrode has been prepared by hydrothermal approach. In this 3D porous carbon skeleton based electrode materials were exhibited the pseudocapacitive performance value of  $1672 \text{ F g}^{-1}$  and the maintained electrode stability up to 3000 cycles at  $5 \text{ A g}^{-1}$  [36]. 3D composite (Graphene/ $\text{Co}_3\text{O}_4$ ) has potential for an array of electrochemical (Supercapacitor and sensor) applications using hydrothermal and CVD methods. In particular, the monolithic free standing electrode, which can be applied for the enzymeless detection ( $<25 \text{ nM}$ ) and the delivered specific capacitance value  $\sim 1100 \text{ F g}^{-1}$  [37]. Generally, the electrochemical properties of the silicone carbide microspheres/birnessite-type  $\text{MnO}_2$  ( $\text{SiC/MnO}_2$ ) composite can employed in supercapacitor applications, the achieved energy storage capacitance value of  $251.3 \text{ F g}^{-1}$  at  $10 \text{ mV s}^{-1}$ . The electrode was tested up to 1000 cycles, the displayed cyclic electrode retention, stability of 94.43 % [38]. The nanofiber morphology and large specific electrode area of vanadium oxide based polypyrrole ( $\text{V}_2\text{O}_5/\text{Ppy}$ ) composite was deposited on carbon cloth by organic-inorganic electro-co-deposition method. The nanofiber composite displayed higher capacitance ( $412 \text{ F g}^{-1}$ ) value and it exhibited good energy storage properties with large potential window ( $-1.4$  to  $0.6 \text{ V vs SCE}$ ) [39].

### 2.3. Conducting polymer

Specifically, core-shell (Fig.3A) and sponge (Fig.3b) like structure of carbon nanotube can be modified with polypyrrole and  $\text{MnO}_2$  have been fabricated by three-different (CVD, electropolymerization and hydrothermal) methods. The demonstrated synergetic effects of CNT-Ppy- $\text{MnO}_2$  electrode, which were exhibited the highest specific capacitance ( $325 \text{ F g}^{-1}$ ) than the CNT- $\text{MnO}_2$ -Ppy ( $241 \text{ F g}^{-1}$ ), i.e. A sponge like structure can act as the good free-standing and excellent cyclic stability electrode for energy storage device applications. Similarly, the other type of electrochemical test has been carried out by EIS, the polymer based sponge electrode was showed obviously decreased the  $R_{CT}$  value than the unmodified electrodes (Fig.3C) [40].

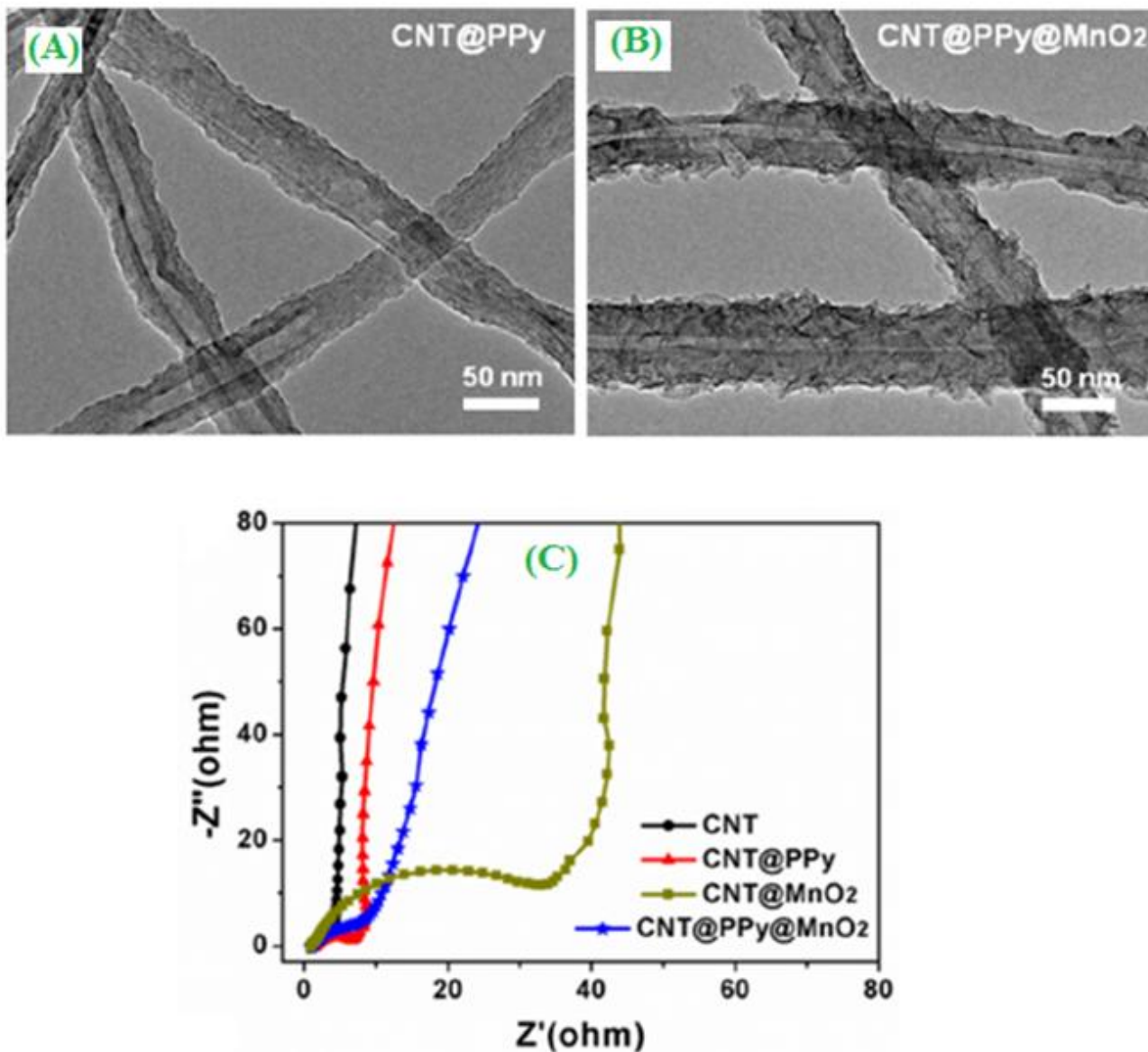


**Figure 3.** TEM images of (A) CNT@PPy sponge, (B) CNT@PPy@MnO<sub>2</sub> sponge and (C) Nyquist plots of the EIS for the four sponges. ("Reprinted with permission from (ACS. Appl. Mater. Interfaces, 6 (2014) 5228). Copyright (2014) American Chemical Society").

Typically, the active graphene-wrapped polyaniline hollow spheres (PANI-HS) modified with electrochemically reduced graphene oxide (ERGO), it can be used as a novel hybrid electrode material for supercapacitor studies. The wrapped electrode can offer an enlarged specific surface area, high electroactive region and shorter diffusion length, the reported energy capacitance value of 614 F g<sup>-1</sup> to 500 cycle's charge-discharge (90 %) durability [41]. An emerging well-aligned CoO and uniform surface polypyrrole (Ppy) array electrode has been used to boost up the pseudocapacitive performance. The synergistic electroactive interaction between CoO and Ppy leads to obtain the highest specific capacitance (2223 F g<sup>-1</sup>). In this type of composite, it has been widely used in aqueous asymmetric capacitance devices, exhibiting the highest power density (~5500 W Kg<sup>-1</sup>) and remarkable cyclic stability (~20000) [42]. While, the thin film porous (Pore size 30-150 nm) of polyaniline-camphor sulphonic acid (PANI-CSA) have been employed as supercapacitive electrode materials for the

obtained the observed capacitance ( $361 \text{ F g}^{-1}$ ), which was more than two order increases than that of pristine PANI electrode [43]. The porous conducting polymer based composite (Polypyrrole/phosphomolybdate) film was prepared by chemical method using tetrahydrofuron (THF) and sodium sulfonate act as porogen. For this kind of polymer based hybrid materials were observed the highest specific capacitance and excellent cyclic electrode stability [44]. The electrochemical activity of polypyrrole/sulfonated graphene (Ppy/SG) composite was higher ( $360 \text{ F g}^{-1}$ ) than that of unmodified sulfonated graphene electrode by charge-discharge method [45]. The most favourable specific surface area ( $94 \text{ m}^2 \text{ g}^{-1}$ ), free standing and flexibility of graphene/polyaniline composite electrode showed a stable and large electrochemical capacitance value of  $233 \text{ F g}^{-1}$  and its tensile strength of  $12.6 \text{ MPa}$  [46].

#### 2.4. Nanocomposite

The functionalized based-graphene nanocomposites were most commonly used as a great potential electrode for supercapacitor applications. Cyclic voltammetry was used as an electrochemical technique, which can be analyzed at different hydrogen-induced exfoliated functionalized graphene based composites for supercapacitor [47]. Among these electrodes, graphene-petched CNT/MnO<sub>2</sub> nanocomposite have attracted for the great attention of high performance ( $486.6 \text{ F g}^{-1}$ ) flexible asymmetric capacitive behaviour, because the operated voltage of  $1.6 \text{ V}$  with an energy density of  $24.8 \text{ Wh kg}^{-1}$  [48]. The interesting carbon based multi-walled carbon nanotube (MWCNT), which can be modified with cellulose nanofiber by electro spinning and deacetylation methods. The demonstrated nanocomposite reduced their activation energy from  $\sim 230$  to  $\sim 180 \text{ KJ mol}^{-1}$ , the surface area also increases after the addition of MWCNT. The leading nanofiber based composite reported the electrochemical capacitance from  $105$  to  $145 \text{ F g}^{-1}$  [49]. Among the various capacitive electrode materials, a low-cost and easily fabricated ternary (Graphene-single-walled carbon nanotube-poly(3-methylthiophene)) nanocomposite can be used as a high performance capacitive electrode. The electrodes were exhibited good electrochemical interaction between graphene, SWCNT and poly(3-methylthiophene) and it was confirmed by FT-IR spectrum, UV-visible and Raman spectroscopic analysis. This type of ternary nanocomposites were reported good electrical conductivity ( $4.68 \text{ S cm}^{-1}$ ) and their achieved the highest specific capacitance value of  $561 \text{ F g}^{-1}$  [50]. Silver nanoparticle coated polyaniline with MWCNT nanocomposite have been regarded as inexpensive electrode materials for high performance energy storage devices. The Ag-nanocomposite showed better electrochemical interactions between Ag, PANI and MWCNT, the possible electrochemical properties of power density ( $4185 \text{ W kg}^{-1}$ ) and energy densities ( $187.73 \text{ Wh kg}^{-1}$ ) have been evaluated by the following equations:

$$P = E/t \quad (2)$$

$$E = 1/2(CV^2) \quad (3)$$

Where C is specific capacitance ( $\text{F g}^{-1}$ ), V-is operating voltage, t-is time (Seconds), E is energy density ( $\text{Wh kg}^{-1}$ ) and P is power density ( $\text{W kg}^{-1}$ ) [51]. More recently, a three-dimensional nano flake of ternary (reduced graphene oxide) rGO/CNTs/MnO<sub>2</sub> electrode was usually applied in promising electrode materials for supercapacitor in  $1 \text{ M Na}_2\text{SO}_4$  aqueous solution. The developed ternary

nanocomposite delivered the highest specific capacitance ( $319 \text{ F g}^{-1}$ ) and enhanced the cyclic stability (3000 cycles) [52]. A facile hydrothermal co-deposition method was used to prepare the porous nickel hydroxide-manganese dioxide-reduced graphene oxide ( $\text{Ni}(\text{OH})_2\text{-MnO}_2\text{-RGO}$ ) ternary electrode play an important role in electro capacitive behaviour (Fig.4A).

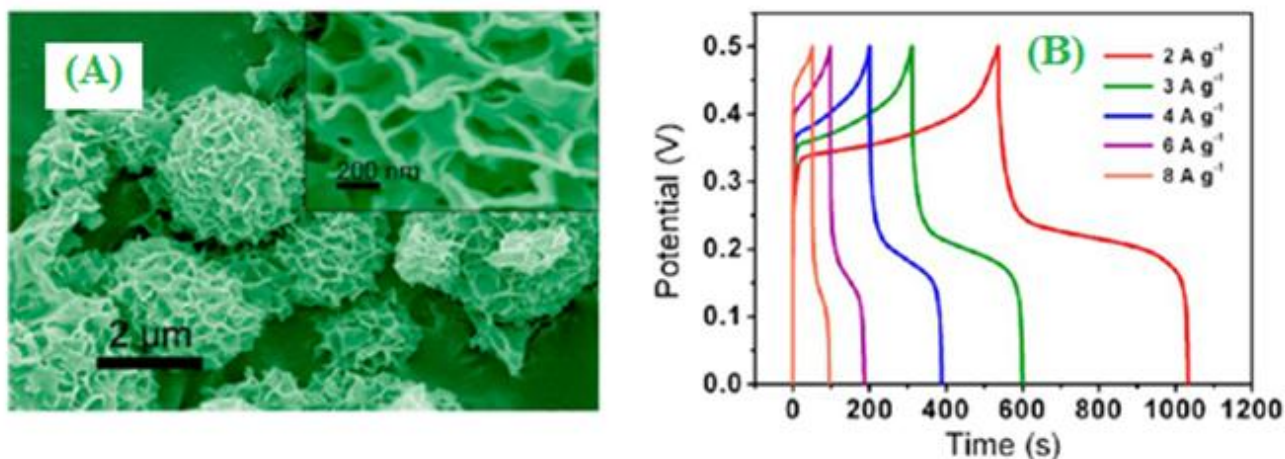


**Figure 4.** (A) SEM image of the  $\text{Ni}(\text{OH})_2\text{-MnO}_2\text{-RGO}$  (B) Galvanostatic discharge curves of  $\text{Ni}(\text{OH})_2\text{-MnO}_2\text{-RGO}$  hybrid sphere-electrode at different current densities. ("Reprinted with permission from (*ACS. Appl. Mater. Interfaces*, 6 (2014) 8621). Copyright (2014) American Chemical Society").

The enhancement in electrochemical capacitance ( $1985 \text{ F g}^{-1}$ ) was ascribed by charge-discharge method (Fig.4B) [53].

### 3. CLASSIFICATION OF SUPERCAPACITORS

#### 3.1. Electrical double layer capacitance (EDLCs)

The new development of energy storable and easily renewable various electrode materials of electrical double layer capacitors have been evaluated by the following equation.

$$C = \frac{\epsilon^* \epsilon_0}{d} A \quad (\text{Eq.4})$$

Where C-is the capacitance,  $\epsilon$  is the dielectric constant of the electrolyte phase,  $\epsilon_0$ -dielectric permitting of the free space. A low-cost source of 3D-ordered mesoporous (3DOM) carbon (Fig.5A Poly(phenol-Formaldehyde\_10) (PF\_10) & B Poly(phenol-Formaldehyde\_40) (PF\_40)) materials prepared by template method. Consequently, the 3DOM carbon materials were extradinarly exhibited for the EDLCs with their high specific capacitance value range of  $146\text{-}178 \text{ F g}^{-1}$  as shown in Fig.5C [54]. The use of multi-walled carbon nanotube (MWCNT)-based EDLCs showed their capacitance value of  $32 \text{ F g}^{-1}$ , whereas by the addition of activated charcoal (AC), substantially increased the higher capacitance value up to  $157 \text{ F g}^{-1}$  [55]. The porous and binder-free carbon nanofibers (CNFs) electrode produced by centrifugal spinning method using polyacronitrile/poly(methyl methacrylate)

(PAN/PMMA) with annealed ( $900^{\circ}\text{C}$ ) fiber diameter of  $7.50 \times 10^2$  nm and the achieved specific capacitance value of  $144\text{ F g}^{-1}$  [56].

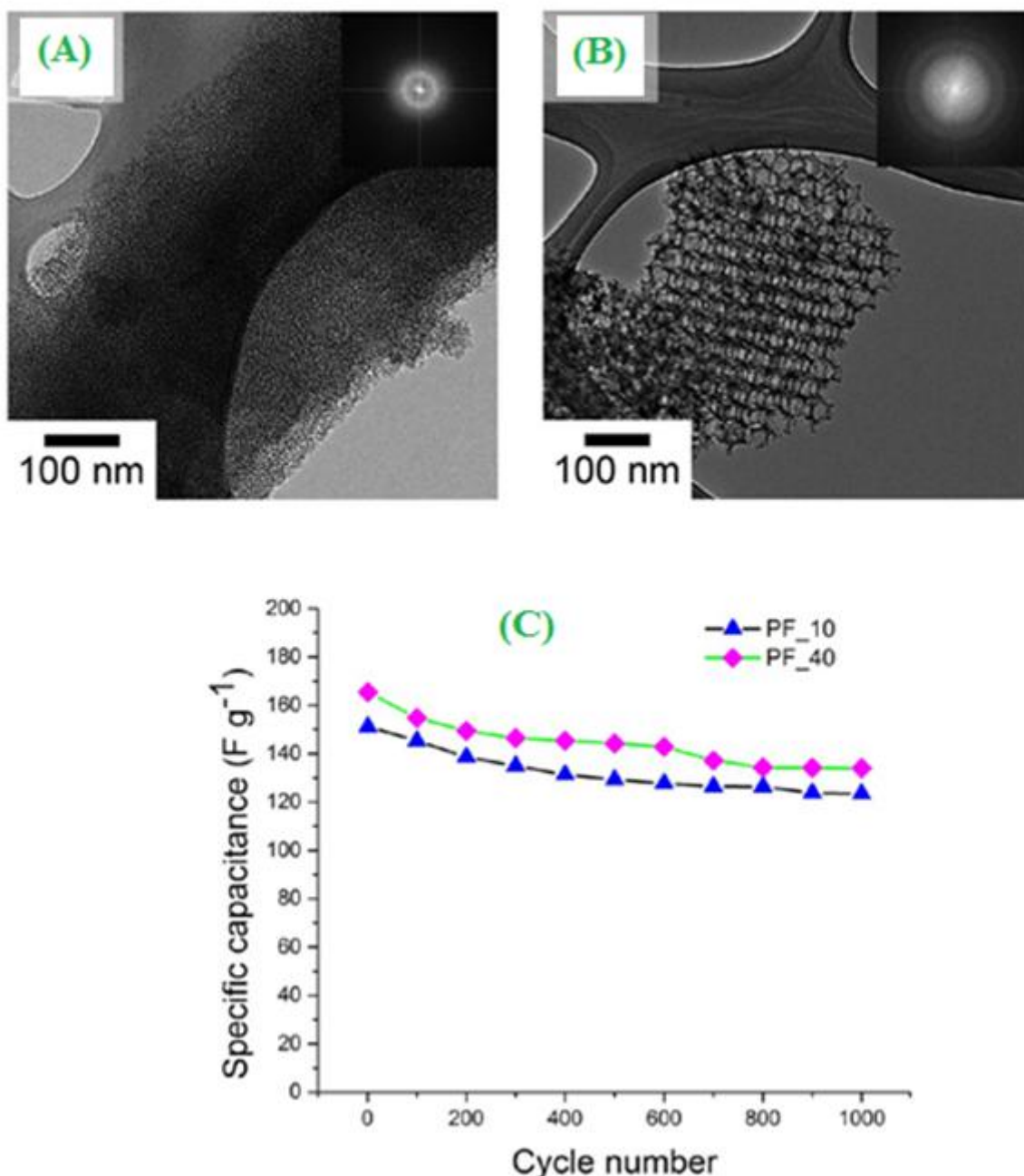


**Figure 5.** (A & B) TEM images and corresponding FFTs of 3D Om (A) PF\_10, PF\_40 carbons and (C) Cycling data for each 3D Om PF carbon electrode in a symmetrical cell. Cells were charged and discharged at  $5.0\text{ A g}^{-1}$ . ("Reprinted with permission from (*Chem. Mater.*, 25 (2013) 4137). Copyright (2013) American Chemical Society").

The most commonly used solvothermal method for the preparation of a novel ultramicro porous carbon nanoparticles (UCNs) in EDLCs, the particles size around 30 nm and their operating high performance capacitance ( $206\text{ F g}^{-1}$ ) stability retention over 5000 cycles [57]. Itoi *et al* [58] used the 3D array zeolite-templated carbon based electrode as a promising energy storage devices in

EDLCs. The multi-connected nanoporous (1.2 nm) capacitor have been analyzed by both gravimetric ( $140\text{-}190\text{ F g}^{-1}$ ) and volumetric ( $75\text{-}83\text{ F cm}^{-3}$ ) methods in  $1\text{ M Et}_4\text{BF}_4$ . The developing of nanoscalable properties of reduced graphene oxide (rGO) as an effective electrochemical application in EDLCs [59]. The most popular chemical vapour deposition technique has been used for the synthesis of single-walled carbon nanotube (SWCNT) electrode showed a remarkable (Specific capacitance) electrochemical behaviour [60].

### 3.2. Hybrid capacitors

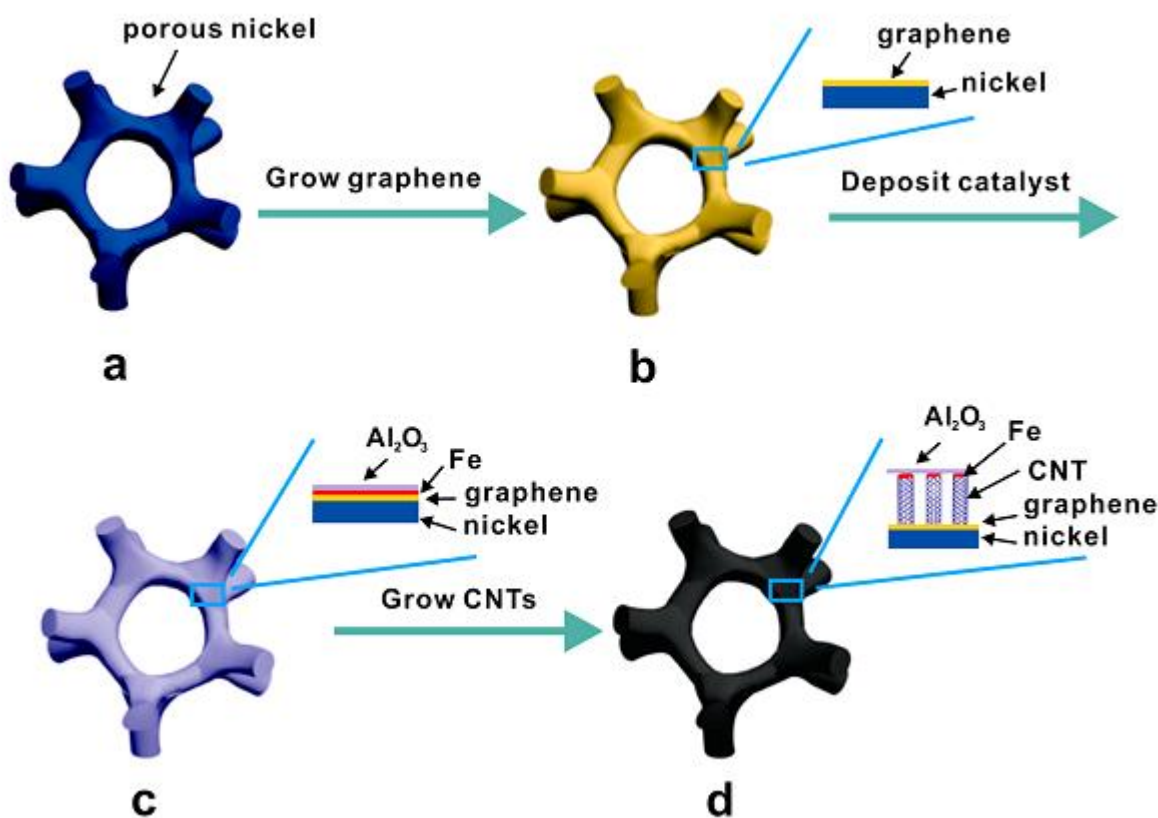


**Figure 6.** Scheme for the synthesis of CNT forests on graphene-porous nickel. (a) The porous nickel substrate. (b) Few-layer graphene is formed on the porous nickel by a CVD method. (c) Fe and Al<sub>2</sub>O<sub>3</sub> are sequentially deposited on the graphene using e-beam evaporation. (d) A CNT forest is directly grown from the graphene surface while lifting the Fe/Al<sub>2</sub>O<sub>3</sub> catalyst layer. ("Reprinted with permission from (*ACS Nano*, 7 (2013) 58). Copyright (2013) American Chemical Society").

Figure.6. Shows the scheme for the preparation of a 3D graphene-CNT multifunctional hybrid electrode by CVD and e-beam evaporation methods on a nickel, for the investigations of its supercapacitor energy efficient oriented technologies [61]. The most present system of Si-C-O glass, which can be modified with activated carbon positive electrode performed favorably with an EDLC. The energy densities of lithium hybrid capacitors (LHC) were exhibited three times higher than that of EDLC [62]. Terasawa *et al* [63] investigated the high performance of hybrid capacitor using nickel peroxide (NiO<sub>x</sub>H<sub>2</sub>O) fabricated with the vapour grown carbon nanofiber (VGCF) and ionic liquids (IL)

(NiO<sub>x</sub>H<sub>2</sub>O/ VGCF/IL) as the electrochemical capacitor in an IL used 1-ethyl-3-methylimidazolium tetrafluoroborate (EMI[BF<sub>4</sub>]). The significant electrochemical and electromechanical properties were observed from the NiO<sub>x</sub>H<sub>2</sub>O/ VGCF/IL electrode. A possible utilization, carbon containing Li<sub>3</sub>V<sub>2</sub>(PO<sub>4</sub>)<sub>3</sub> (LVP-C) anode and lithium-ion hybrid electrochemical capacitor (Li-HEC) applied with activated carbon (AC) as a cathode. Here, Li-HEC exhibited a remarkable energy density than AC/LVP-C [64]. However, a mild hydrolysis method constructed aqueous hybrid capacitor of activated carbon based TiO<sub>2</sub> (AC/TiO<sub>2</sub>) nanoparticles have an operating cell potential 1.7 V and possessed their higher energy density (9.7 Wh kg<sup>-1</sup>) and power density (563.0 W kg<sup>-1</sup>) [65]. A hybrid capacitor consisting with 3D-MnO/carbon nanosheets array (Anode), on the other hand carbon nanosheets act as the cathode displayed both the energy densities and power densities (184 Wh kg<sup>-1</sup> at 83 W kg<sup>-1</sup> and 90 Wh kg<sup>-1</sup> at 15000 W kg<sup>-1</sup>) over 5000 cycles [66]. The electrochemical test at 10M KOH conditions showed that NiO electrode prepared by galvanostatic anodization method resulted in positive electrode hybrid capacitor specific energy of 16 Wh kg<sup>-1</sup> and their specific power 22.2 kW kg<sup>-1</sup> [67].

### 3.3. Pseudocapacitors

The demonstration of MoO<sub>3</sub> derivative (Ky-MoO<sub>3-x</sub>) has been prepared by using K<sup>+</sup> insertion and hydrothermal method opened up new approach for the developing new kind of electrode materials, which was applied in high volumetric capacitor (305 F cm<sup>-3</sup> at 0.5 A g<sup>-1</sup>) and excellent rate performance (175 F cm<sup>-3</sup> at 100 A g<sup>-1</sup>) [68]. Zhou *et al* [69] pointed out the best electrochemical performance (1313 F g<sup>-1</sup> at 1A g<sup>-1</sup>), when different morphological structural (Porous, planar dendrite, bundle and flower-like tube etc.) oriented and large surface area of Ni-Sn alloy. Preparation of a well-defined mesoporous MnO<sub>2</sub> nanosheet array on Ni foam from one-step electro deposition and low-temperature thermal processes have been used as the effective method, which were pseudo capacitive behaviour evaluated by cyclic voltammetry technique. The nanosheet reported specific capacitance values of 201, 150, 122, 105 and 96 F g<sup>-1</sup> at the applied current densities like 1, 5, 10, 15 and 20 A g<sup>-1</sup> [70]. In order to extend the study of anodic deposition of 3D porous vanadium oxide has been focused on the unique power characteristic (167 F g<sup>-1</sup> at 25 mV s<sup>-1</sup>) pseudocapacitor applications [71]. Sonochemically synthesized BiPO<sub>4</sub> nanocrystals used in pseudocapacitor applications, the optimized electrolyte (pH = 7) and ultrasonic power (60% Instrument power) displayed superior specific capacitance value of 1052 F g<sup>-1</sup> at 2 mV s<sup>-1</sup> [72]. Graphene (Graphene/carbon nanotubes/manganese oxide) based nanocomposite has been investigated an advanced electrode materials for high energy density asymmetric pseudocapacitor. Moreover, the interconnected nanocomposite electrode exhibited higher electrode surface area and excellent specific capacitance (964 F g<sup>-1</sup> at 1A g<sup>-1</sup>) [73]. Gong *et al* [74] studied NiCo<sub>2</sub>O<sub>4</sub> nanowire arrays, which were delivered higher areal capacitance (6 F cm<sup>-2</sup>), good specific capacitance (1132 F g<sup>-1</sup>) and remarkable electrode stability.

### 3.4. Ultracapacitors

Ultracapacitor is one of the most conventional energy storage devices like cost-effective electrode, high-surface area, high power density, worldwide performance and long-durability etc. A

high performance ultracapacitive nature of nitrogen-doped graphene based electrode has been synthesized via a simple plasma route. The resulted ultracapacitor value of  $\sim 280 \text{ F g}^{-1}$ , which was 4 times higher than that of pristine graphene [75]. An environmentally friendly, time-efficient and cost-effective holey graphene (h-graphene) was synthesized by a scalable approach. In this type of catalyst-free and chemical free two-dimensional nano hole h-graphene reached the highest capacitance of  $54 \text{ F cm}^{-3}$  at  $3 \text{ A g}^{-1}$  for 10000 cycles [76]. The versatile flake structure of  $\alpha\text{-Co(OH)}_2/\text{Co}_3\text{O}_4$  asymmetric ultracapacitor displayed the high specific capacitance ( $583 \text{ F g}^{-1}$ ) at  $1 \text{ A g}^{-1}$ , maximum power density ( $290 \text{ W kg}^{-1}$ ) and energy density ( $22.4 \text{ Wh kg}^{-1}$ ) was evaluated [77]. Liu *et al* [78] used the planar ultracapacitor of hydrous ruthenium oxide nano rod, which can be fabricated with the integral stack layer of gold and titania (hRuO<sub>2</sub> NRGT) electrode by both photolithography and sputter coating methods. The capacitive behaviours were measured the output energy ( $295 \text{ }\mu\text{J}$ ) and the power output was  $1.23 \text{ }\mu\text{W}$ . The ferromagnetic nature and controlled morphology of pure magnetite ( $\text{Fe}_3\text{O}_4$ ) electrode has been shown their exhibited ultracapacitor's specific capacitance value of about  $97 \text{ F g}^{-1}$  [79]. The application of high BET surface area ( $3100 \text{ m}^2 \text{ g}^{-1}$ ) carbon aerogel is an electrode material in high energy ultracapacitor, the tested voltage range 0-1.8 V. The electrode based devices, the highest specific capacitance value obtained so far was  $156 \text{ F g}^{-1}$  with a stability of 20000 [80]. The multi-layered of conducting polymer film (Poly(3,4-ethylenedioxythiophene) and polypyrrole) has been deposited on the steel uncoated and coated with octanethiol. The high performance ultracapacitor displayed their capacitance value of  $80 \text{ F g}^{-1}$  [81].

#### 4. VARIOUS SYNTHESIS METHODS

The most promising  $\text{NiCo}_2\text{O}_4$  multiple hierarchical structures have been developed by hydrothermal method and it can be used as promising electrode materials for supercapacitor ( $2623.3 \text{ F g}^{-1}$ ) applications [82]. The biopolymer assisted  $\lambda\text{-MnO}_2$  nanoparticles have been prepared by green approach method using 0.1M manganese nitrate and 0.1M dextrose [83]. In a self-assembled method,  $\text{MoO}_3$  nano belt was sonochemically irradiated for 4h and the *in situ* polymerization of 0.2 mL pyrrole for the fabrication of  $\text{MoO}_3/\text{PPy}$  nanocomposite, which it act as the hybrid electrode materials in super capacitor studies [84]. The high specific capacitance ( $802.5 \text{ F g}^{-1}$ ) achieved  $\gamma\text{-MnS/rGO}$  composite has been prepared in Teflon lined autoclave the subjected temperature of  $190^\circ \text{ C}$  and the product was dried at  $60^\circ \text{ C}$  for 12 h [85]. The plane arrangement face centre cubic (FCC) crystals of  $\text{Co}_3\text{O}_4$  and tetragonal  $\text{RuO}_2$  based ( $\text{RuO}_2:\text{Co}_3\text{O}_4$ ) thin film electrode, which was prepared by a non-aqueous spray pyrolysis method [86]. Hummers and electrospinning methods can be used for the preparation of a high capacitive (Graphene oxide/ $\text{V}_2\text{O}_5$ ) composite nanofiber electrode [87]. A large surface area and wire based graphene/tantalum electrode has also found extensive application in high performance energy storage devices and it was synthesized by chemical vapour deposition (CVD) [88]. Another, face-to-face electrostatic self-assembled method involved the fabrication of high quality graphene based- $\text{MnO}_2$  (Graphene/ $\text{MnO}_2$ ) nanocomposite electrode in electrochemical applications [89].

## 5. ELECTRODE SURFACE AREA (BET)

You groups have developed a three-dimensional hierarchical porous carbon CNT-graphene ternary all-carbon foams (3D-HPCFs) electrode exhibited large surface area ( $1286 \text{ m}^2 \text{ g}^{-1}$ ) and outstanding capacitive electrode materials for next generation energy devices (Fig.7) [90]. In the case of supercapacitor, the oxidized form of graphite-graphite oxide core-sheath fiber electrode could possess a high surface area ( $255 \text{ m}^2 \text{ g}^{-1}$ ) and its pore size around 5.5 nm. This graphite based electrode undergoes good faradic electrochemical behaviour and it yielded high specific capacitance ( $140 \text{ F g}^{-1}$ ) and good cyclic stability (3000) [91]. In order to calculate the optimized as-prepared and electrodeposition of  $\text{Co}_3\text{O}_4/\text{RuO}_2$  calcined electrode ( $53.1 \text{ m}^2 \text{ g}^{-1}$ ), which was dramatically improved their current density ( $10 \text{ A g}^{-1}$ ), rate capacity and retained (96 %) maximum capacitance [92]. The microbe bundled morphological based carbons (MTBCs) have been synthesized from Paulownia sawdust (PS).

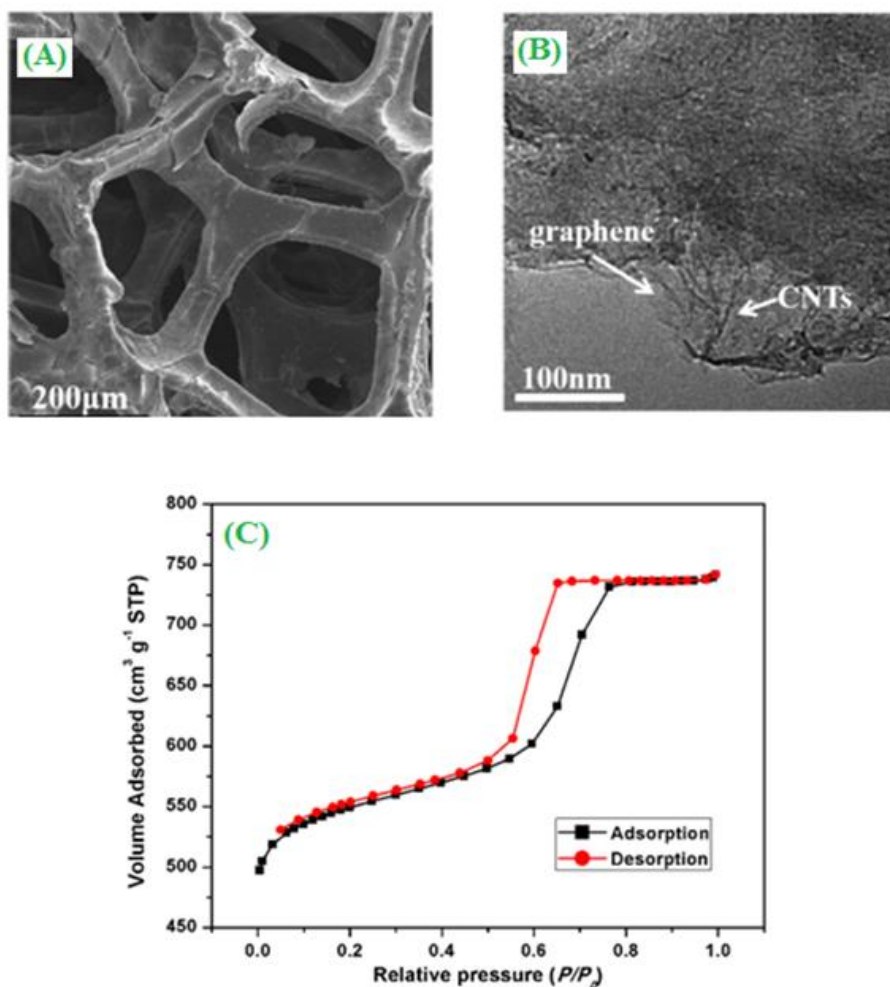


**Figure 7.** (A) SEM image of 3D-HPCFs, (B) TEM image of 3D-HPCFs and (D)  $\text{N}_2$  sorption isotherms of 3D-HPCFs. ("Reprinted with permission from (*ACS. Appl. Mater. Interfaces*, 6 (2014) 15302). Copyright (2014) American Chemical Society").

They possess high specific surface area ( $1900 \text{ m}^2 \text{ g}^{-1}$ ) from  $\text{N}_2$  adsorption-desorption isotherm studies and also the reported electrochemical properties of  $227 \text{ F g}^{-1}$  at  $2 \text{ mV s}^{-1}$  [93]. The better performance and promising electrode materials of mesoporous carbon nanofibers ( $1424 \text{ m}^2 \text{ g}^{-1}$ ) were synthesized from phenolic resol with alumina anodic membrane electrode [94]. In this context, a special attention has been applied for the fabrication of phosphorous nitrogen contained graphene nanosheets (NGs) for the remarkable enhanced ( $7.6$  to  $244.6 \text{ F g}^{-1}$ ) supercapcitive performance by the addition of phosphoric acid ( $\text{H}_3\text{PO}_4$ ). In this  $\text{H}_3\text{O}_4$  treated active NGs electrode morphological and electrode surface area were analyzed by HRTEM, XRD and BET isotherm etc [95]. Among these, Hausmannite tetragonal structures of  $\text{Mn}_3\text{O}_4$ /amorphous carbon ( $\text{Mn}_3\text{O}_4/\text{AC500}$ ) electrode play an important role in supercapacitor ( $522 \text{ F g}^{-1}$ ) applications. The observed  $\text{Mn}_3\text{O}_4/\text{AC500}$  electrode measured BET specific surface area of  $38.4 \text{ m}^2 \text{ g}^{-1}$  and exhibited better pore volume for electrochemical usage [96]. Chou *et al* [97] have used carambola  $\gamma\text{-MnO}_2$  nanoflake electrode for the evaluation of the electrode surface area by using the following equation:

$$S_E = \frac{C_{dl}}{C_d} \quad (5)$$

Where  $S_E$  is electrochemical active surface area,  $C_{dl}$  is double layer capacitance and  $C_d$  is constant capacitor.

## 6. ROLE OF MORPHOLOGY IN SUPERCAPACITOR

### 6.1. Flower morphology

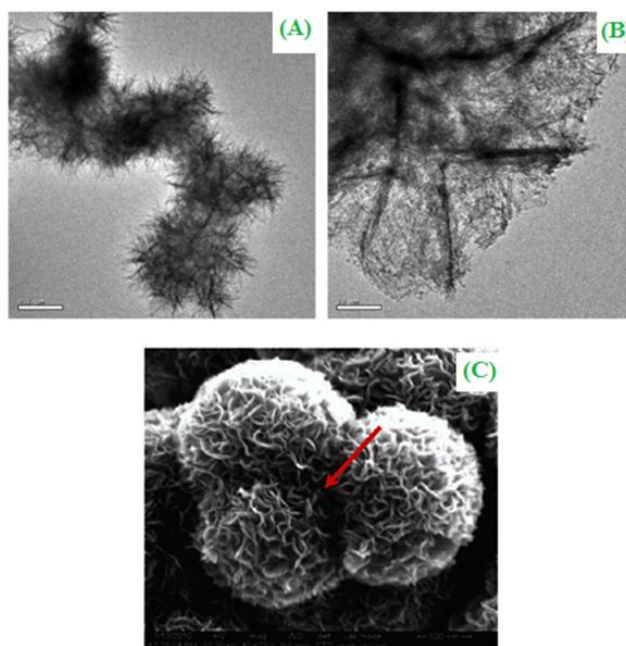


**Figure 8.** (A) & (B) Low and high-resolution HRTEM images of NiO sample showing flower like morphology (C) high-resolution FESEM images of NiO sample. ("Reprinted with permission from (*ACS. Appl. Mater. Interfaces*, 3 (2011) 2063). Copyright (2011) American Chemical Society").

Meher *et al* [98] have used two different flower morphological nickel oxide (NiO) electrodes have been prepared by both microwave-assisted and reflux methods. Fig.8.(A&B) showed the two different low and high-resolution HRTEM images of NiO nanoflakes formed flower-like morphology and the high-resolution FESEM image of NiO agglomerated flower morphology (Fig.8C). Here, microwave assisted synthesized NiO electrode showed highest specific capacitance ( $370 \text{ F g}^{-1}$ ) value than that of reflux synthesized NiO ( $101 \text{ F g}^{-1}$ ). Similarly, Wang *et al* [99] made a controlled synthesis of high surface area and novel flower like structure of the carbon mesoporous structure showed that the estimated specific capacitance value of  $200 \text{ F at } 1 \text{ A g}^{-1}$ , which was 2.5 times lower ( $79 \text{ F}$ ) than carbon electrode. Moreover, a three-dimensional  $\text{SnO}_2$  nanoflower has been widely reported as the good electrode materials in supercapacitor applications. The synthesized nanoflowers width around  $5 \text{ nm}$  and the expected enhanced capacitance value of  $410 \text{ mF cm}^{-2}$  [100]. Template-free microwave-assisted heating (MAH) was one of the approaches for the fabrication of a suitable porous flower shaped binary metal oxide ( $\text{NiCo}_2\text{O}_4$ ) microspheres electrode. The developed electrode was boosting their electrochemical behaviour ( $1006 \text{ F g}^{-1}$ ) and long cycle life (1000 cycles) [101]. Considerably, a novel development of poly(3,4-ethylenedioxyppyrrrole) can be enfolded with  $\text{Bi}_3\text{S}_3$  (PEDOT/ $\text{Bi}_3\text{S}_3$ ) nanoflower electrode was prepared by electropolymerization method. The highly focus on new strategies of nanoflower electrode was improve their capacitive ( $329 \text{ F g}^{-1}$ ) and delivered high power density [102]. Wang *et al* [103] have prepared a cost-effective and surfactant free porous  $\beta\text{-Co(OH)}_2$  with flower morphologies and used the synthesized porous electrode for a high performance super capacitor ( $416 \text{ F g}^{-1}$ ) applications for about 500 cycles (93 % retention). Similarly, Tang *et al* [104] synthesized nickel cobalt hydroxide ( $\text{Ni}_x\text{Co}_{(1-x)}(\text{OH})_2$ ) nanoflower electrode by a facile-free hydrothermal method. The possible ammonia complexation Ni/Co ratio with improved their asymmetric capacitance properties.

## 6.2. Nanofiber morphology

The most widely used accepted nitrogen-functionalized carbon nanofiber electrode, which can be modified with nickel hydroxide (N-CNF/ $\text{Ni(OH)}_2$ ) electrode was synthesized by Cai and his co-workers. The fiber material has maximum specific capacitance ( $\sim 1045 \text{ F g}^{-1}$ ) and excellent cyclic stability (Fig.9) [105]. The mesoporous ( $10 \text{ to } 50 \text{ nm}$ ) and large surface area ( $500 \text{ m}^2 \text{ g}^{-1}$ ) of polyacrylonitrile/poly(methylacrylate) (PMMA) fiber electrode provided the highest specific capacitance ( $128 \text{ F g}^{-1}$ ) in  $6\text{M KOH}$  [106]. The hierarchical network architecture of  $\text{Co}_3\text{O}_4$  nanowire deposited on carbon fiber paper electrode, the nano net electrode showed ideal capacitive ( $1124 \text{ F g}^{-1}$ ) behaviour and improved their rate capacity and cyclic stability [107]. Mi *et al* [108] have obtained polyaniline nanofiber electrode by template method using ferric chloride and ammonium persulfate as the oxidant. The fabricated PANI nanofiber diameter around  $20\text{-}40 \text{ nm}$ , most importantly the displayed electrode capacitance value of  $428 \text{ F g}^{-1}$  in  $1\text{M H}_2\text{SO}_4$ . Similarly, a three-dimensional and free-standing of polyaniline was fabricated on porous carbon nanofiber electrode as promising capacitive materials due to its higher power density and excellent specific capacitance [109]. The interconnected nanofibers have also been proved to be suitable electrode matrices for supercapacitor applications and it exhibited 100 % cyclic stability [110]. Excellent performance of supercapacitor was studied in

various activation methods for prepared porous activated carbon fiber electrode (ACF). It was observed that, HP20-1/3-900 triangle shaped electrode displayed more capacitance ( $180 \text{ F g}^{-1}$ ) than the normal one [111].

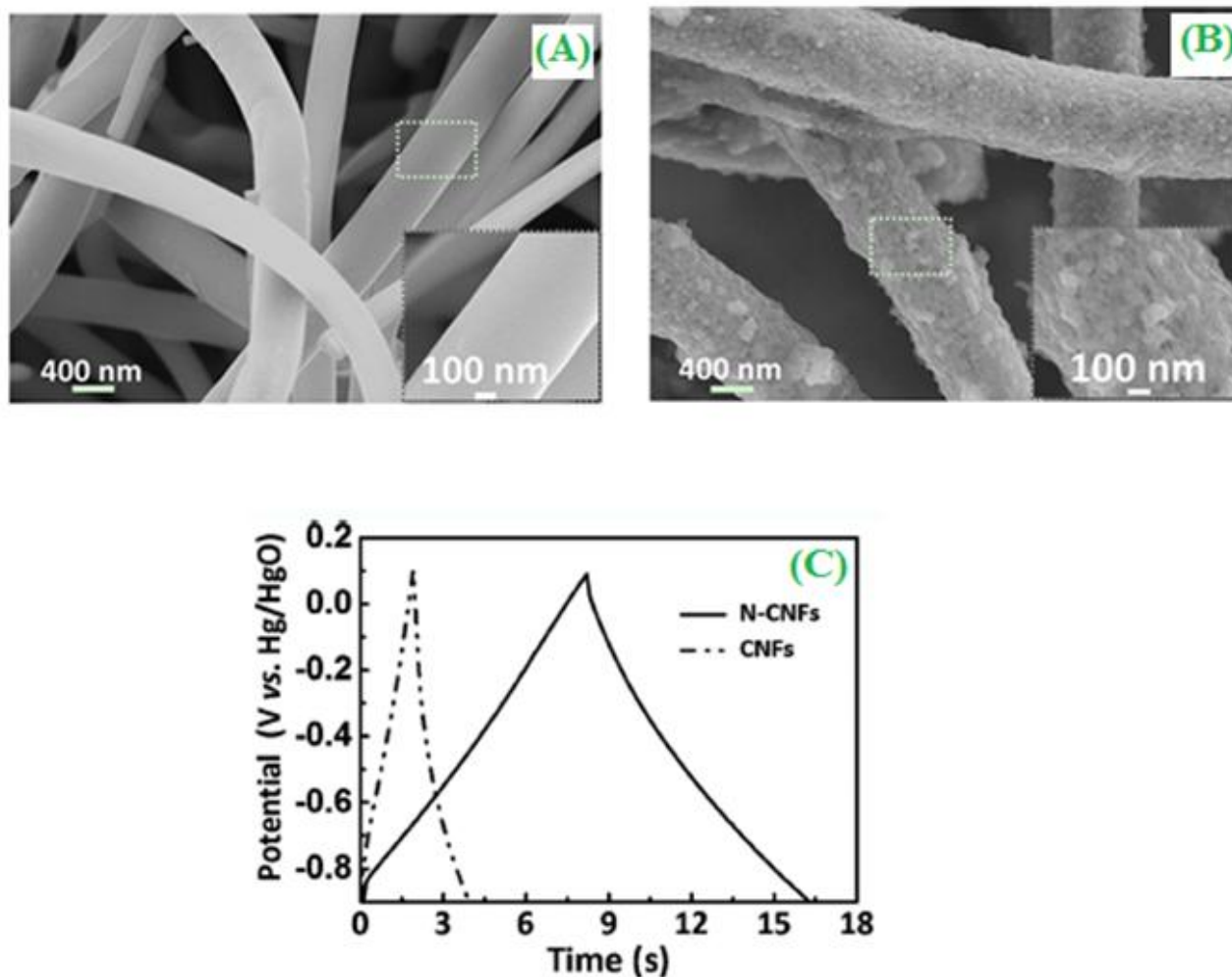


**Figure 9.** (A) & (B) SEM images of CNFs and N-CNFs (C) Typical GCD curves of CNFs and N-CNF electrodes at a current density of  $20 \text{ A g}^{-1}$ . ("Reprinted with permission from *ACS. Appl. Mater. Interfaces*, 7 (2015) 14946). Copyright (2015) American Chemical Society").

### 6.3. Nanowire electrode

Currently, the high performance of metal oxide based  $\text{Co}_3\text{O}_4/\text{NiO}$  nanowire array can make use of the conductive substrate for the attractive capacitor application. The demonstrated self-assembled nanowire array electrode exhibited  $853 \text{ F g}^{-1}$  for 6000 cycles [112]. The highest electrochemical retention (96.1 %) capacitance of a free-standing 3D Ni@NiO nanowire membrane electrode has been fabricated by simple filtration and thermal annealed methods. Fig.10.(A&B) shows the SEM and TEM images of crosssectional embedded Ni@NiO nanowire. The electrochemical analysis of Ni based nanowire membrane electrode at different annealed temperatures was recorded at  $50 \text{ mV s}^{-1}$  in 1M

KOH solution (Fig.10.C). In this type of nanowire membrane capacitor, which can be used as a new class of energy storage materials for wonder rate capability and high power density [113].

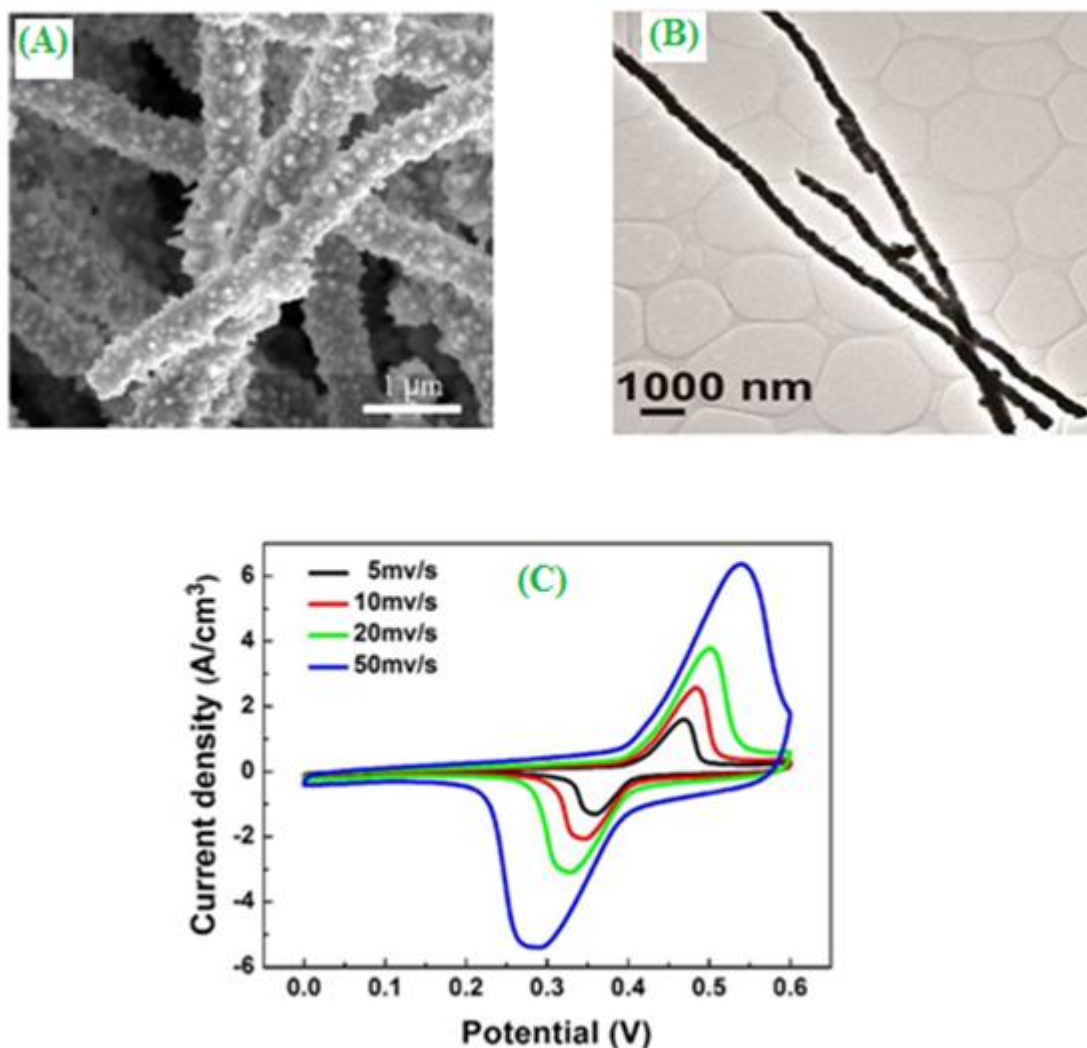


**Figure 10.** (A) SEM image of Cross-sectional SEM image of the ultrathin 3D mesoporous free-standing Ni@NiO nanowire membrane (B) TEM image of three Ni@NiO nanowires and (C) CV curves of the sample with an annealing temperature of 350 °C at different scan rates ranging from 5 to 50 mV s<sup>-1</sup>. ("Reprinted with permission from (*ACS. Appl. Mater. Interfaces*, 6 (2014) 13627). Copyright (2014) American Chemical Society").

The hierarchical nanocomposite has been combined with polyaniline nanowire array and graphene oxide nanosheets (PANI/GO). Nevertheless, the electrochemical conductivity of hierarchical nanocomposite showed better specific capacitance (555 F g<sup>-1</sup>) [114]. Particularly, large-scale uniform  $\alpha$ -Co(OH)<sub>2</sub> nanowire arrays were found to have high specific capacitance and excellent capacitance retention during the galvanostatic charge-discharge method [115]. Xia *et al* [116] investigated the supercapacitor devices on a new type of 3D porous thin film form of graphite foams, conducting polymers and metal oxide nanowire (GF/Co<sub>3</sub>O<sub>4</sub>/PEDOT-MnO<sub>2</sub>) composite, which was prepared by electropolymerization method. The usefulness of newly formed ternary alkali metal based copper

chalcogenide  $\text{KCu}_4\text{Se}_8$  nanowire electrode has been demonstrated in supercapacitor ( $25.3 \text{ F g}^{-1}$ ) studies. By the fabrication of  $0.1 \text{ Mg V}_2\text{O}_5$  nanowire on  $\text{KCu}_4\text{Se}_8$  surface, the specific capacitance also enhanced up to  $93.7 \text{ F g}^{-1}$  at  $10 \text{ mV s}^{-1}$  [117].

#### 6.4. Nanorod electrode

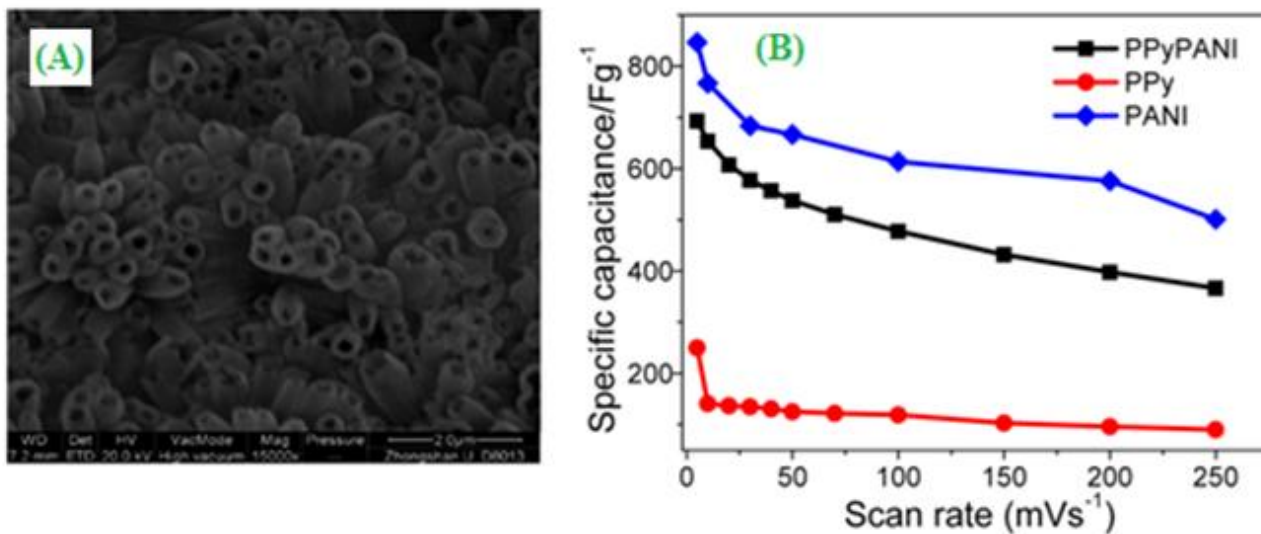


**Figure 11.** (A) SEM image of PPy/PANI DNTAs (B)  $C_{sp}$  values of PPy/PANI DNTAs, PPy nanotube arrays and PANI nanotube arrays as a function of scan rate. ("Reprinted with permission from (ACS. Appl. Mater. Interfaces, 6 (2014) 642). Copyright (2014) American Chemical Society"). (Ref<sup>118</sup>)

Zinc oxide nano rod array was electrodeposited by the galvanostatic electrolysis method at  $1.0 \text{ mA cm}^{-2}$  for 90 minutes ( $70^\circ \text{ C}$ ). In this nano rod arrays were polymerized with  $0.01 \text{ M}$  pyrrole. Finally, it can further  $0.1 \text{ M}$  aniline was electro polymerization on  $\text{ZnO/PPy}$  nano rod arrays. Fig.11. Shows that the analytical (SEM) and electrochemical (Cv) studies of PPy/PANI double-walled nanotube arrays (DNTAs). The electro fabricated PPy/PANI nano rod arrays electrode showed good specific capacitance ( $693 \text{ F g}^{-1}$ ) and the cyclic electrode performance up to 1000 cycles [118]. Li *et al* [119] found by use of scanning electron microscope (SEM) that showed the interesting morphology of polyaniline nanorod-graphene nano ribbon (PANI/GNRs) composite. They found the reported composite had highest specific capacitance and large scale production of energy storage devices. Xu *et al* [120] have standard the electrochemical behavior of  $\text{Co}_9\text{S}_8$  array positive electrode and  $\text{Co}_3\text{O}_4@\text{RuO}_2$  nanosheet array as an anode material by the autoclave method at  $120^\circ \text{ C}$  for 10h in a hot oven. The electrochemical techniques including cyclic voltammetry and charge-discharge methods have been applied for investigation of their capacitance. The electro active of the cobalt oxyhydroxide ( $\text{CoOOH}$ ) nano rod electrode towards the supercapacitor analysis by charge-discharge method, the observed capacitance value of  $198 \text{ F g}^{-1}$  and its retention (83 %) stability for 5000 cycles [121]. The substrate like  $\text{Bi}_2\text{S}_3$  nano rod based graphene composite has also been proved to be suitable host matrices for both photo electrochemical and supercapacitor applications [122]. In particularly, manganese molybdate ( $\text{MnMoO}_4$ ) nano rods have been prepared by sonochemical method. The

electrode has been found to offer the great scope of the maximum obtained ( $168.32 \text{ F g}^{-1}$ ) specific capacitance value [123].

### 6.5. Nano porous electrodes

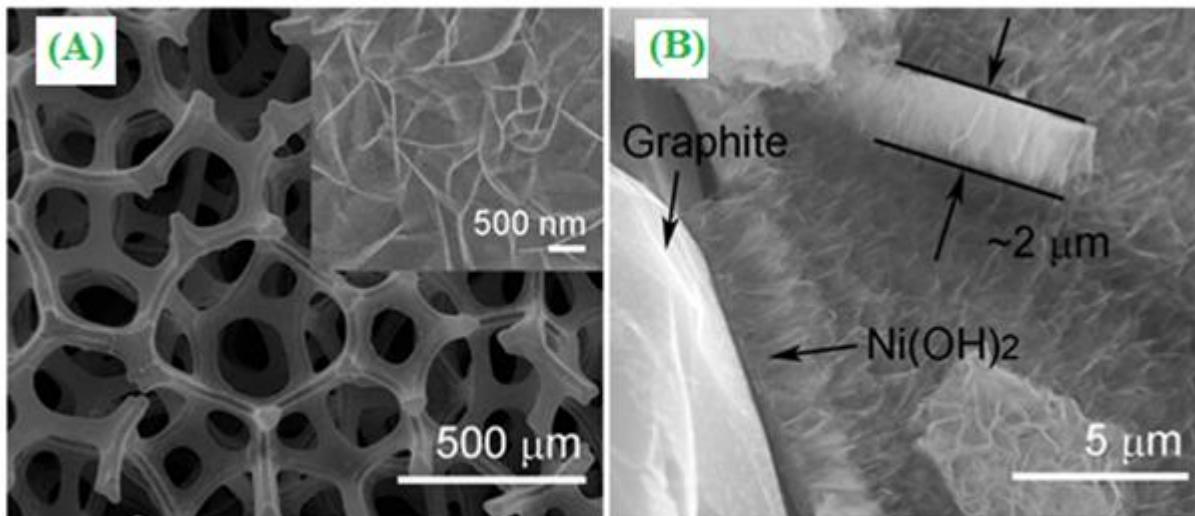


**Figure 12.** (A) SEM images of the  $\text{Ni(OH)}_2/\text{UGF}$  composite (B) Cross-sectional view of the composite (C) Galvanostatic charge-discharge curves at various current densities. ("Reprinted with permission from (*ACS Nano*, 7 (2013) 6237). Copyright (2013) American Chemical Society").

Ji *et al* [124] have reported that the hydrothermal prepared nano porous  $\text{Ni(OH)}_2$  thin film can be modified with 3D ultrathin-graphite foam (UGF) (Fig.12.A&B) ( $\text{Ni(OH)}_2/\text{UGF}$ ) composite caused a

high conductive network and enhanced the electron transport properties of cost-effective energy storage devices (Fig.12.C). Although, the controlled morphologies of nanoporous  $\text{Co}_3\text{O}_4$ , cubic spinel  $\text{Co}_3\text{O}_4$  with spherical (0D) and hexagonal platelet (2D) were used them supporting matrices for supercapacitor applications. From the electrochemical (Cyclic voltammetry, EIS and charge-discharge) analysis of  $\text{Co}_3\text{O}_4$  hexagonal platelet presented the highest capacitance ( $\sim 476 \text{ F g}^{-1}$ ) value than  $\beta\text{-Co(OH)}_2$ ,  $\text{CoO}$  and spherical  $\text{Co}_3\text{O}_4$  [125]. Saravanakumar *et al* [126] have studied the supercapacitive behaviour of interconnected vanadium pentoxide ( $\text{V}_2\text{O}_5$ ) nanoporous network electrode by means of the achieved annealed ( $300^\circ \text{ C}$ ) samples capacitance value of  $316 \text{ F g}^{-1}$  and their respective energy density of  $43.8 \text{ Kh kg}^{-1}$ . The uses of fine tuning supercapacitive nanoporous carbon electrode materials were exhibited with different pore diameters (3 to 6 nm). The highest performance of capacitance values were significantly increased from 108 to  $186 \text{ F g}^{-1}$  [127]. A high pore volume ( $0.87 \text{ cm}^3 \text{ g}^{-1}$ ) and large BET surface area ( $1322.5 \text{ m}^2 \text{ g}^{-1}$ ) of nitrogen doped manganese oxide coated nano porous carbon (Carbon-2:1-Mn) electrode can greatly enhanced their electrochemical performance ( $564.5 \text{ F g}^{-1}$ ) [128]. Thus, exploiting nano porous carbon has been extracted from waste coffee beans and they attracted their porosity to improve their capacitive behaviour ( $368 \text{ F g}^{-1}$ ) [129].

## 7. ELECTROCHEMICAL ANALYSIS

### 7.1. Cyclic voltammetry

Nanowire based manganese oxide-tin oxide ( $\text{MnO}_2/\text{SnO}_2$ ) composite provided better electronic conductivity and the observed specific capacitance value was calculated by cyclic voltammetric method.

$$C = \frac{Q}{\Delta V m} \quad (6)$$

Where  $C$  is the specific capacitance ( $\text{F g}^{-1}$ ),  $m$ -is the mass of the electrode (g),  $Q$ -is the average charge (C) and  $\Delta V$  is the applied potential window (V) [130]. Cai *et al* [131] reported the preparation of  $\text{NiMoO}_4$  nanospheres and nano rods by a facile hydrothermal method (Fig.13.A).

The active metal oxide electrode could provide different specific capacitance values of 974.4, 920.8, 875.5, 859.1 and  $821.4 \text{ F g}^{-1}$  at different current densities 1, 2, 4, 6 and  $10 \text{ A g}^{-1}$  (13.B). A uniform and nanoporous ( $\sim 130 \text{ nm}$ )  $\text{MnO}_2$  has been deposited by electrochemical method. The specific capacitance studies were evaluated by cyclic voltammetry method, the modified stainless steel mesh-ITO nanowire and  $\text{MnO}_2$  nanofiber electrode showed the highest specific capacitance ( $667 \text{ F g}^{-1}$ ) [132]. A self-assembled dispersion polymerization (SSDP) method also led to the formation of highly porous conductive polyaniline-camphour sulphonic acid (PANI/CSA) electrode, which was more than two order specific capacitance values higher than that of PANI electrode evaluated by cyclic voltammetrically [133].

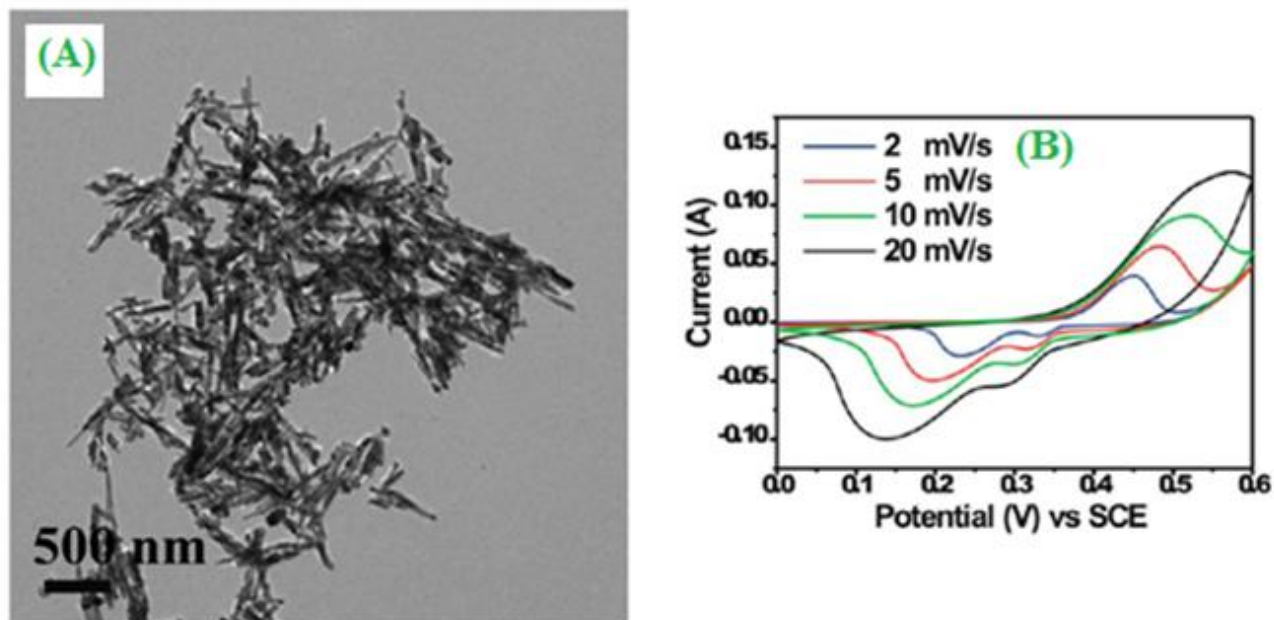


**Figure 13.** (A) TEM images of the NiMoO<sub>4</sub> nanorods (B) Cyclic voltammetry (CV) curves of NiMoO<sub>4</sub> nanospheres and nanorods in a 3 M KOH aqueous solution. ("Reprinted with permission from (*ACS. Appl. Mater. Interfaces*, 5 (2013) 12905). Copyright (2013) American Chemical Society").

Sol-gel is a viable method to form hierarchically porous carbons (HPCs) electrode, which was cyclic voltammetrically employed for the evolution of electrochemical capacitance behaviour at various scan rates of 1-10 mV s<sup>-1</sup>. Thus, HPCs which showed a highest specific capacitance value of 41 F g<sup>-1</sup> at 20 mV s<sup>-1</sup> in 6.0M KOH [134]. The ultrahigh supercapacitor of lacey reduced graphene oxide nanoribbon (LRGONR) electrode has been investigated in aqueous, non-aqueous and ionic electrolytes etc., The most widely accepted symmetric capacitor showed the power intensity value of 807 W kg<sup>-1</sup> in aqueous medium [135]. The new capacitance oriented conducting polymer based manganese dioxide (Poly(3,4-ethylenediothiophene) (PEDOT)-polyaniline (PAN)) nanocomposite have been investigated. Moreover, the composite could improve their widespread capacitor, which was evaluated through cyclic voltammetry at different scan rates (2-20 mV s<sup>-1</sup>) [136].

## 7.2. Charge-discharge

### 7.2.1. At various electrodes

Yao *et al* [137] have fabricated at different ratios based carbon nanotube SEM images of (CNT)/microporous carbon core-shell (KA-CNT/carbon-5, KA-CNT/carbon-10, KA-CNT/carbon-25 and KA-CNT/carbon-50) nanocomposites (Fig.14.A-D).

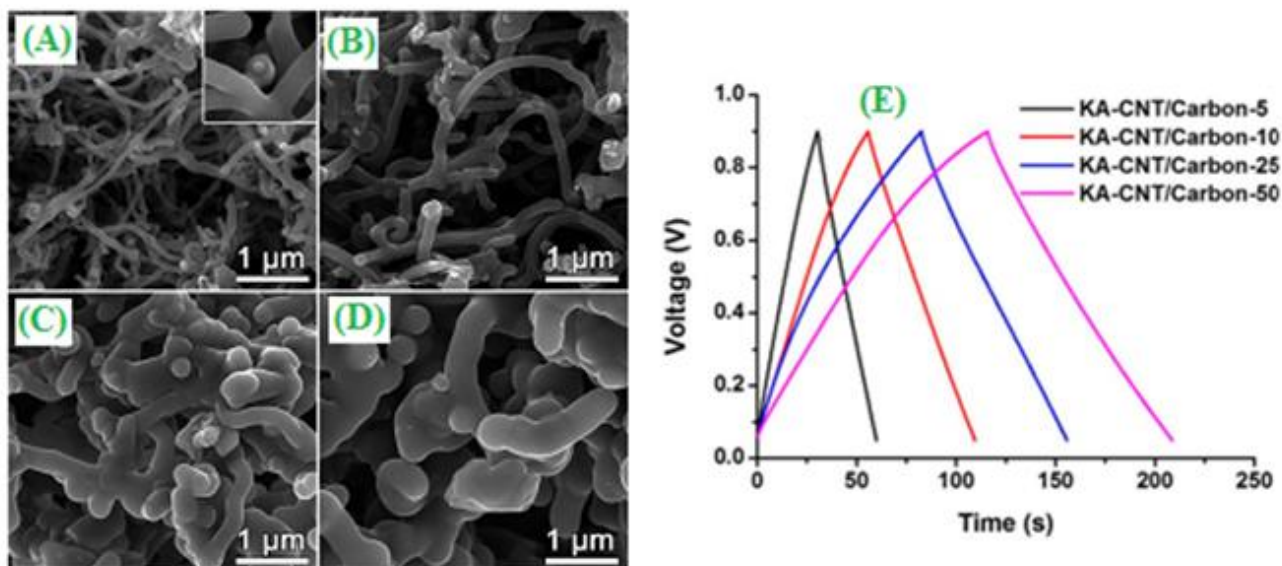


**Figure 14.** SEM images of the KOH-activated KA-CNT/carbon core-shell nanocomposites (A) KA-CNT/carbon-5 (B) KA-CNT/carbon-10 (C) KA-CNT/carbon-25 (D) CNT/carbon-50 and (E) Electrochemical performance of the KOH-activated KA-CNT/carbon nanocomposites by galvanostatic charge-discharge curves at  $1 \text{ A g}^{-1}$ . ("Reprinted with permission from (*ACS. Appl. Mater. Interfaces*, 7 (2015) 4817). Copyright (2015) American Chemical Society").

These kinds of different ratios, carbon based composites have been optimized by galvanostatic charge-discharge method (Fig.14.E) The optimized high-surface area of KA-CNT/carbon-50 core-shell nanocomposite reported the highest specific capacitance value and excellent retention (75 %) cyclic stability. Liu *et al* [138] synthesized hollow spherical nitrogen-rich porous carbon shells via carbonization structure controlled by high temperature ( $700$ ,  $800$  and  $900^\circ \text{C}$ ) methods. In these thermal conditions, nitrogen rich, hollow spheres ( $800^\circ \text{C}$ ) modified with porous carbon content (NPC-800) electrode revealed the highest specific electrode surface area and excellent specific capacitance. The three different graphene (Hybrid graphene/ $\text{MnO}_2$  (GM), graphene/ $\text{MnO}_2$ /CNT (GMC) and graphene/ $\text{MnO}_2$ /poly(3,4-ethylenedioxythiophene)-poly(styrenesulfonate) (PEDOT:PSS) (GMP)) based composite electrodes were extensively studied for supercapacitor applications. By these three-dimensional composites, GMP achieved the highest specific capacitance ( $\sim 380 \text{ F g}^{-1}$ ) and good retention capacitance up to 3000 cycles [139]. In particularly, nanostructured hexagonal boron nitride (h-BN)/reduced graphene oxide (RGO) composite matrices have been found to offer great scope for this electrochemical (Specific capacitance  $\sim 824 \text{ F g}^{-1}$ ) applications [140]. The high performance supercapacitors of polyaniline based carbon paper modified with polyninyl alcohol (PANI-carbon paper-PVA- $\text{H}_2\text{SO}_4$ ) assisted composite electrode have been reported. The displayed electrode device capacitance value of  $647 \text{ F g}^{-1}$  with their areal capacitance of  $1 \text{ F cm}^{-2}$  [141].

### 7.2.2. At various current densities

The development of flexible, oriented light weight, low-cost and high performance three-dimensional graphene network based  $\text{MnO}_2$  (3D-Graphene/ $\text{MnO}_2$ ) composite has been

electrochemically (Galvanostatic charge-discharge) performed with different current densities such as 0.3, 0.5, 1.0 and 4.0 mA cm<sup>-2</sup> as shown in Fig.15 [142].

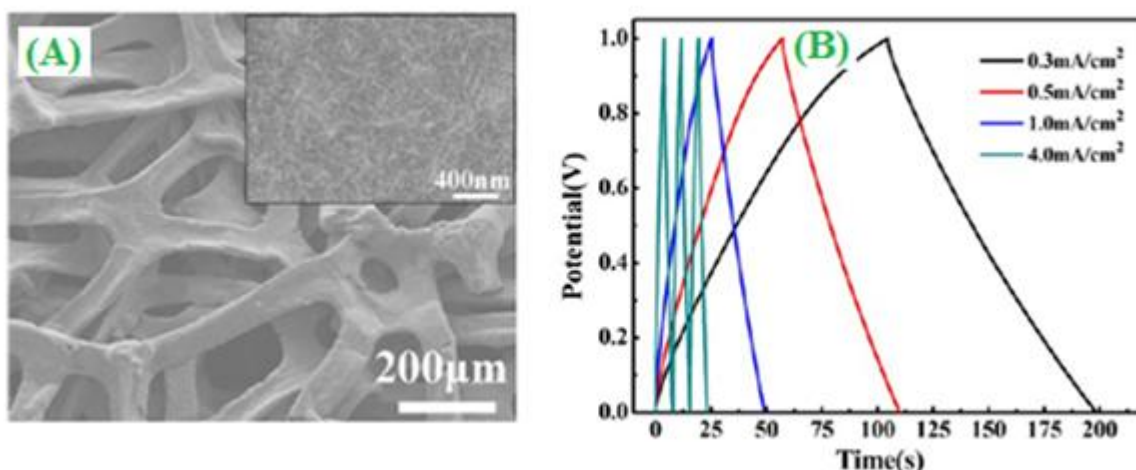


**Figure 15.** (A) SEM images of uniform coating of MnO<sub>2</sub> inside and outside the 3D graphene networks (B) Galvanostatic charging-discharging curves of the flexible supercapacitor device at different current densities. ("Reprinted with permission from (*ACS Nano*, 7 (2013) 174). Copyright (2013) American Chemical Society").

The microwave-assisted and CVD induced in situ methods for the fabrication of polyaniline nanofiber coated graphite composite considered as a promising electrode materials in high performance energy storage devices. The demonstrated PANI based composite was exhibited the different capacitance values like 2136 for 1A g<sup>-1</sup> and 425 F g<sup>-1</sup> for 20 A g<sup>-1</sup> [143]. A high electrode surface area (466 m<sup>2</sup> g<sup>-1</sup>) chemically reduced borane reduced graphene oxide (B-rGO) nanoplate electrode showed the reasonable capacitive (200 F g<sup>-1</sup>) properties and long duration cyclic (4500) stability [144]. Zinc tin oxide (ZnSnO<sub>4</sub>) (ZTO) nanowire diameter of 80 nm have been deposited over manganese oxide and carbon nanofiber (MnO<sub>2</sub>/ZTO/CMF) hybrid composite evaluated in both cyclic voltammetry and chronoamperometry (At various current densities) [145]. Recently, the unique and attracted ZnO@Co<sub>3</sub>O<sub>4</sub> core-shell heterostructures have been synthesized by a facile and cost-effective hydrothermal method. In this core-shell heterogeneous structure showed a remarkable capacitance value of 857.7 F g<sup>-1</sup> at 1A g<sup>-1</sup> [146]. The charge-discharge (At different current densities) studies of supercapacitor based on the boron doped porous carbon (BPCs) electrode with high surface area (1800 m<sup>2</sup> g<sup>-1</sup>) was obtained from carbon dioxide at mild conditions [147].

### 7.3. Electrochemical impedance spectroscopy (EIS)

The nano pod dimension morphology of cetyltrimethylammonium bromide (CTAB) assisted hexagonal platelet Co(OH)<sub>2</sub> has been fabricated on graphene (Co(OH)<sub>2</sub>/graphene) hybrid composite. The fabricated materials were characterized by FT-IR, XRD, FESEM and their electrochemical analysis by Cv, charge-discharge and EIS etc. From the Nyquist plot, the highly conducting Co(OH)<sub>2</sub>/graphene composite was greatly reduced their R<sub>CT</sub> and its diffusion resistance [148]. Kotal *et*

al [149] fabricated the nanofiber based morphologies of polyaniline-carbon composite by conventional method (Fig.16.A-D).

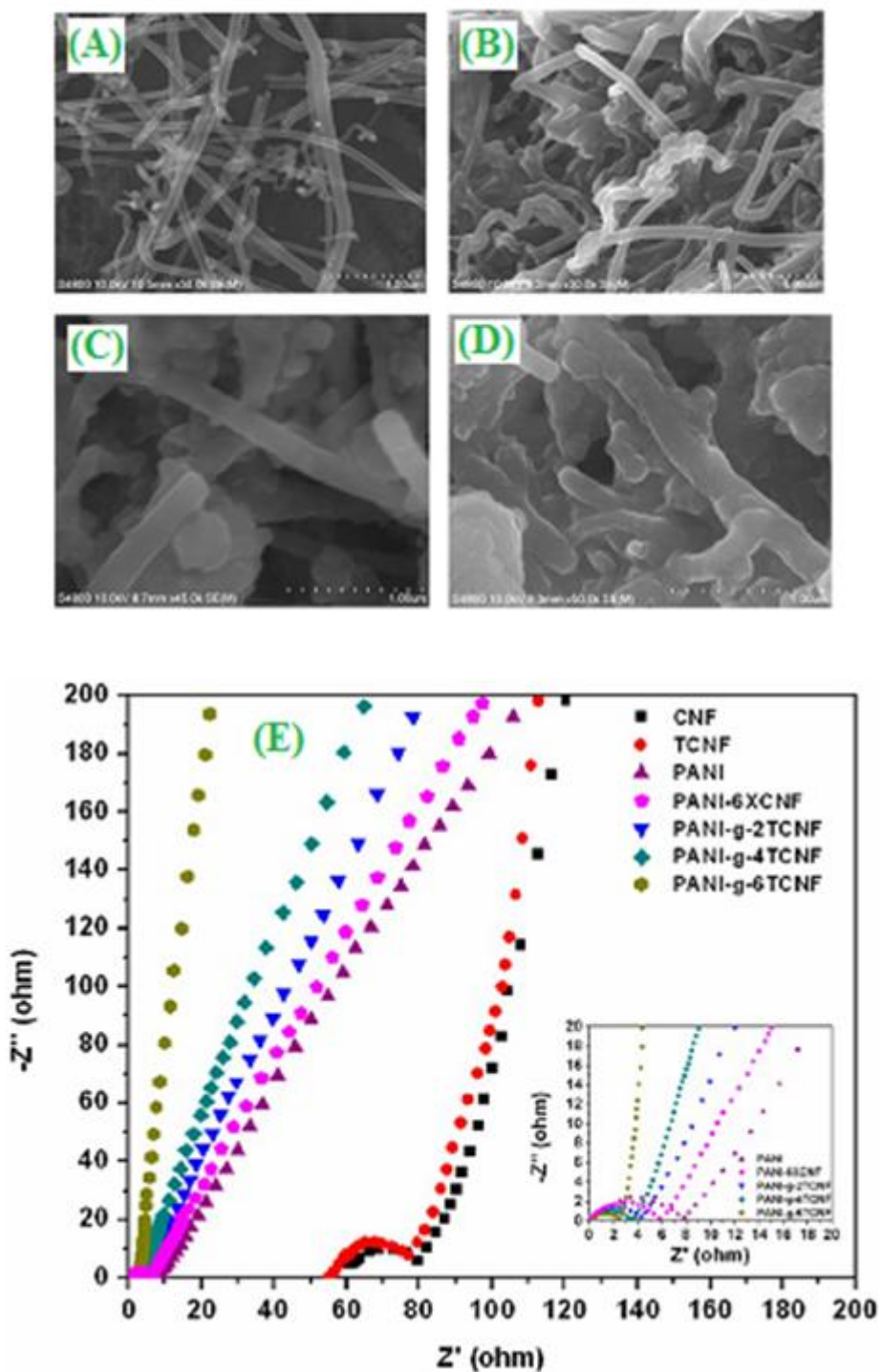


**Figure 16.** FESEM images of (A) CNF, (B) XCNF, (C) TCNF, and (D) a PANI-g-TCNF composite containing 6 wt % TCNF (E) Nyquist plots recorded from 105 to 0.001 Hz with an ac amplitude of 5 mV for CNF, TCNF, PANI, PANI-6XCNF, and PANI-g-TCNF composites containing 2, 4, and 6 wt % TCNF. ("Reprinted with permission from (ACS. Appl. Mater. Interfaces, 5 (2013) 8374). Copyright (2013) American Chemical Society").

The suggested electrodes have been optimized by EIS, PANI-g-TCNF composite reported lower interfacial  $R_{CT}$  than that of PANI, TCNF and CNF (Fig.16.E). For the interesting dye-sensitized photo-supercapacitor of poly(3,4-(2',2'-diethylpropylenedioxythiophene)) (PProDOT-Et<sub>2</sub>) thick film electrode was used as a photoelectric energy storage device. Notably, the specific capacitance also can be estimated from the impedance plot.

$$-Z'' = \frac{1}{C_E} (2\pi f)^{-1} \quad (7)$$

Where  $-Z''$  is the imaginary impedance and  $f$  is the frequency in Hz [150]. A high porosity of nitrogen-doped graphene aerogel (NGA) has been improved their outstanding capacitive (223 F g<sup>-1</sup>) properties and long durability in 1M H<sub>2</sub>SO<sub>4</sub>. The as-prepared 3D porous NGA network, which was electrochemically evaluated by EIS [151]. The free-standing sub-3nm Co<sub>3</sub>O<sub>4</sub> nanofilm can be obtained by the substrate free hydrothermal method. The electrochemical tested nanofilm electrode was obtained the ultra high capacitance value of 1400 F g<sup>-1</sup> [152]. The most promising sponge-like 3D graphene nano architectures showed the normalized specific capacitance value of 16.2 μF cm<sup>-2</sup> at 0.1 A g<sup>-1</sup> [153]. The EIS analysis of 3D interconnected vertically aligned MnO<sub>2</sub> nanoplate was deposited on the nickel foam (MnO<sub>2</sub>-NF) electrode in neutral Na<sub>2</sub>SO<sub>4</sub> solution. However, the  $R_{CT}$  value of asymmetric supercapacitor has been tested for before and after cyclic experiments by using ZS<sub>imp</sub> Win software [154].

## 8. FACTOR AFFECTING OF THE SUPERCAPACITOR

### 8.1. IR drop

Synthesis of a simple and scalable laser-induced graphene (LIG) electrode has been fabricated by laser induction polyimide sheets. The galvanostatic charge-discharge curve was obtained a triangular shape with voltage drop due minimize the internal and contact resistance. The fabricated device exhibited the areal capacitance value of >9 mF cm<sup>-2</sup> at 0.02 mA cm<sup>-2</sup> [155]. Lim *et al* [156] prepared an active device of polyethyleneterphthalate (PET) film applied in high performance micro supercapacitors (MSCs). The usage of the charge-discharge method has been applied for the optimization of PET columbic efficiency values (97 and 94 %). In this remarkable charge-discharge reversibility, which was indicated the voltage (IR) drop potential to be 0.052 and 0.089 V respectively. Another one interesting Li-ion based capacitor (LIC) was evaluated by Cao and his co-workers [157]. However, LIC has been made with activated carbon, hard carbon and stabilized lithium metal powder (SLMP). In this loaded SLMP electrode materials were slightly IR voltage dropped during the electrolysis of both low and high voltages. By supporting of EIS analysis, IR voltage was directly related to the internal resistance of LIC. Tevi *et al* [158] used charge-discharge method of poly(p-phenyleneoxide) as an electrode materials for the investigations of drop voltage curve and reduced the leakage current (~78 %). Chen *et al* [159] prepared tin-oxide based reduced graphene oxide (SnO<sub>2</sub>/rGO) composite using a dynamic self-assembled method, which showed their both highest gravimetric and volumetric capacitances were 310 F g<sup>-1</sup> and 180 F cm<sup>-3</sup>. Unmodified rGO electrode

dynamic processes dropped into the target solution, after the modification of SnO<sub>2</sub>/rGO aerogel showed good specific capacitance and excellent energy storage devices.

### 8.2. Influencing parameters for supercapacitor

The unique and surface edged morphologies of conjoined nanomaterials have been used as a new kind of electrode materials for prominent capacitor (224 F g<sup>-1</sup>) application than that of graphene sheet/MWCNT electrode, these were clearly explained scroll structure had open structure and MWCNT exhibit closed one [160]. Luo *et al* [161] used a porous graphene electrode materials explored the mechanical and electrical conductance properties with various hole defects. The nitrogen-doped graphene materials, thermal stability hole edge, which was calculated by the computational equations.

$$E_F^L = \left( E_{C_xN_y} - xE_C - \frac{Y}{2} E_{N_2} \right) / L \quad (8)$$

Where  $E_{C_xN_y}$  is the energy of the system with a hole,  $E_C$  is the energy per C atom in perfect graphene,  $E_{N_2}$  is the energy of an isolated N<sub>2</sub> molecules etc., The calculated porous nitrogen doped graphene diameter value of 4.2-10 Å and it was exhibited better performance energy storage device in capacitor applications. A well designed, constructed carbon nanotube mesh based polyaniline (CNT/PANI) composite has been synthesized by in situ chemical method.

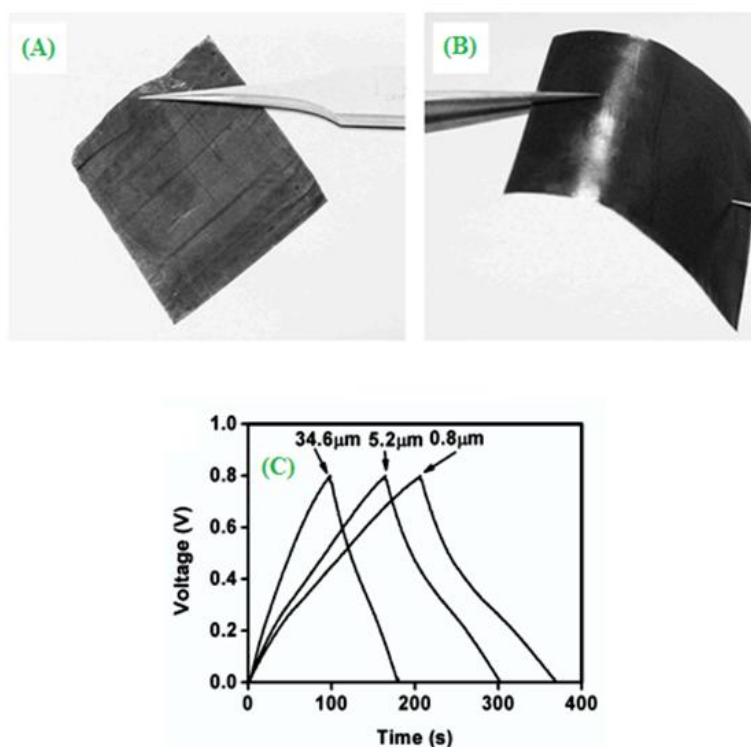


**Figure 17.** (A) & (B) Digital photographs of the well-constructed CNT mesh/PANI with the thickness of 0.8 and 17.4 μm (C) Electrochemical measurement results of well-constructed CNT mesh/PANI with different electrode thickness constant current charging-discharging curves at 1 A g<sup>-1</sup>. ("Reprinted with permission from (*J. Phys. Chem. C*, 116 (2012) 26185). Copyright (2012) American Chemical Society").

Fig.17(A&B) shows the two different thicknesses (0.8 and 17.4  $\mu\text{m}$ ) of digital photographs of CNT mesh/PANI composite, they (34.6, 5.2 and 0.8  $\mu\text{m}$ ) were optimized by a constant current charge-discharging technique (Fig.17.C). The controlled electrode thickness was electrochemically influenced by the capacitance, power density and energy density etc., The resulted optimized 5  $\mu\text{m}$  thickness electrode achieved higher specific capacitance and higher power density ( $9.0 \text{ kW kg}^{-1}$ ) [162]. The worse asymmetric supercapacitor reversibility of  $\text{Ni}(\text{OH})_2$ , after the addition of activated carbon,  $\text{Ni}(\text{OH})_2/\text{AC}$  electrode considered as a balanced charge occur at  $80 \text{ A g}^{-1}$  and the applied potential voltage value of 1.6 V for the improvement of higher electrochemical energy storage devices [163].

### 8.3. Annealing effect

The development of N/P-co-doped thermally ( $800^\circ \text{C}$  for 2h) reduced graphene oxide (N/P-TRGO) has been synthesized by Hummer's method using  $(\text{NH}_4)_3\text{PO}_4$ . The wrinkled layer structure of TRGO showed their electrochemical behavior of  $165 \text{ F g}^{-1}$  and excellent cyclic stability ( $>80\%$ ) [164]. Zhu *et al* [165] reported a facile hydrothermal method ( $180^\circ \text{C}$ ) derived 1D hierarchical tubular  $\text{MnO}_2$  nanostructure electrode using carbon nanofiber (CNF) was used as a sacrificial template. The optimized  $\text{MnO}_2$ -180 electrode, which was electrochemically, tested with charge-discharge method, the resulted highest specific capacitance value of  $315 \text{ F g}^{-1}$  at  $0.2 \text{ A g}^{-1}$ .

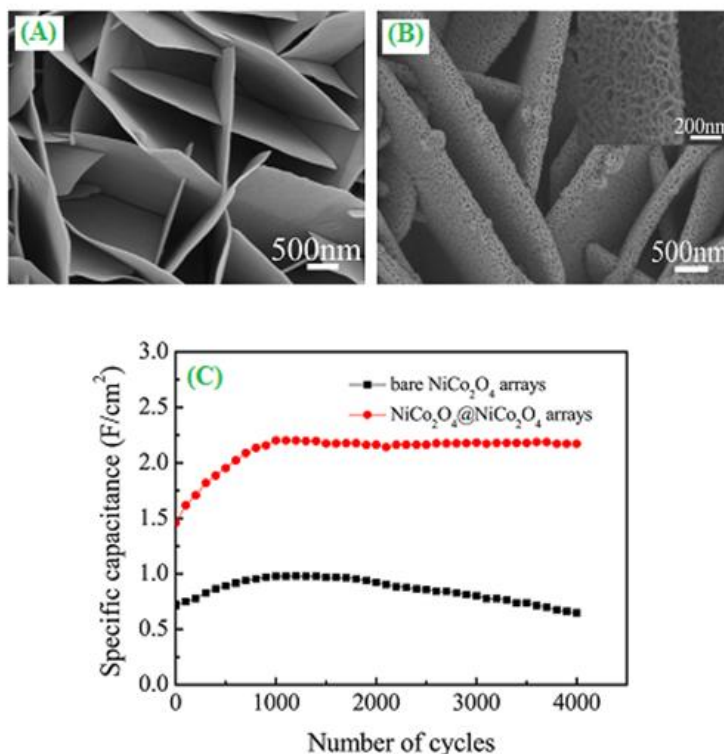


**Figure 18.** SEM images of (A) the bare  $\text{NiCo}_2\text{O}_4$  nanoflake array and (B) the  $\text{NiCo}_2\text{O}_4@ \text{NiCo}_2\text{O}_4$  core/shell nanoflake array grown on Ni foam substrate (C) Areal specific capacitance as a function of cycle number of the bare  $\text{NiCo}_2\text{O}_4$  nanoflake and  $\text{NiCo}_2\text{O}_4@ \text{NiCo}_2\text{O}_4$  core/shell nanoflake. ("Reprinted with permission from (*ACS. Appl. Mater. Interfaces*, 5 (2013) 8790). Copyright (2013) American Chemical Society").

More efficient study of nickel template, high quality of graphene has been prepared by atmospheric pressure chemical vapour deposition method (APCVD). The optimized temperature (650° C) demonstrated the highest specific capacitance (203.4 F g<sup>-1</sup>) and higher energy density (40.9 Wh kg<sup>-1</sup>) in KOH [166]. More recently, Feng *et al* [167] used Co<sub>3</sub>O<sub>4</sub> microspheres (At low temperature hydrothermal method) as an electrode with the exhibited different specific capacitance values were 850, 780, 700 and 630 F g<sup>-1</sup> at various current densities like 1, 2, 4 and 8 A g<sup>-1</sup>. Among the discussed annealed materials, free-standing CNTs grown on carbon film, which were annealed at various temperatures at 500, 600 and 700° C and their estimated film diameters of 72.7 ± 33, 111.9 ± 34 and 183.9 ± 52 nm. The free-standing optimized annealed (600° C) electrode produced the highest specific capacitance value of 484.34 F g<sup>-1</sup> [168].

## 9. CYCLIC STABILITY

Iron oxide supported nitrogen-doped graphene oxide (Fe<sub>2</sub>O<sub>3</sub>/N-rGO) hydrogels were used as the electrode materials for supercapacitors; they exhibited high performance specific capacitance (618 F g<sup>-1</sup>) and good cyclic durability even after 5000 (56.7 % retention) cycles [169]. A novel method for the preparation of reduced graphene oxide (rGO) can be wrapped with polyaniline (PANI) nanowire on nitrogen-doped carbon fiber cloth (eCFC). The hierarchical symmetric capacitor rGO/PANI/eCFC composite displayed an enhanced the specific capacitance (1145 F g<sup>-1</sup>), which was used higher than that of PANI/eCFC and GO/PANI/eCFC. The flexible and binder-free composite achieved only 94 % retention cyclic stability over 5000 cycles [170]. Novels NiCo<sub>2</sub>O<sub>4</sub>@ NiCo<sub>2</sub>O<sub>4</sub> core-shell array electrodes (Fig.18(A&B)) are of great interest in electrochemical capacitor applications. From the electrochemical analysis, the reported highest capacitance value of 2.20 F cm<sup>-2</sup> and their retained (98.6 %) stability up to 4000 cycles (Fig.18.C) [171]. Simple one-step solvothermal methods also lead to the formation of copper ferrite nanoparticle attached graphene nanosheet (CuFe<sub>2</sub>O<sub>4</sub>. GN) from 0.01M CuCl<sub>2</sub> precursor solution by the addition of FeCl<sub>3</sub>.6H<sub>2</sub>O. The discussed electrochemical (576.6 F g<sup>-1</sup>), rate performance a cyclic stability (1000 cycles) has been optimized by charge-discharge method [172]. Butt and co-workers [173] reported a novel hierarchical nanospheres (NHNs) ZnV<sub>2</sub>O<sub>4</sub> electrode by template free method, the observed capacitance properties of 360 F g<sup>-1</sup> at 1 A g<sup>-1</sup>. A 3D-NiO/ultrathin derived graphene (UDG) hybrid electrode have been widely investigated as the capacitive electrode materials, they produced the highest specific capacitance (425 F g<sup>-1</sup>) and good cyclic retention (90 %) stability over 2000 charge-discharge cycles [174].

## 10. CONCLUSIONS

Most of the electrochemical energy storage devices are associated with their choosing electrode materials, high specific surface area and surface morphological structure of the molecules. The authors discuss with synthesis methods, different electrode (Carbon, metal oxides, conducting polymers, nanocomposites and various morphological electrodes) materials, various types of capacitors (EDLCs, hybrid capacitors, pseudocapacitors and ultracapacitors) and the optimized electrochemical (Cyclic

voltammetry, galvanostatic charge-discharge and EIS) techniques, etc. Among the reported electrode materials, only nano based electrodes were exhibited ultimate performance in electrochemical capacitors. From the electrode synthesis/preparation/fabrication part, hydrothermal method was used as a viable one and the synthesized materials reported highest capacitance value of  $2623.3 \text{ F g}^{-1}$ . The improvements of supercapacitor parameters were highly focused on specific capacitance, specific power, specific energy and their long-durability of the overall reported literatures electrode materials. Some of the parameters have been affected and influence by the supercapacitor energy storage devices, such as IR drop, electrode thickness, electrode edges and annealing effect etc. Therefore, the published results have provided massive synergetic effect in electrochemical capacitor studies. Further scientific community will develop easily available materials could ultimately obtained low cost, high performance and excellent cyclic stability of supercapacitor devices. Recently, the fabrication of highly oriented (3-dimensional, hierarchical, nanofiber and nano rod shaped) molecules were reported better specific capacitance and ultimate cyclic performance in supercapacitor applications. Provided, the unique morphological structure and uniform electrode pore volumes were displayed better electrochemical properties.

In general, ultra capacitor is one of the most powerful conventional energy storage devices. It can be used as environmentally friendly, time efficient and worldwide performance capacitors. By the electrochemical analysis, cyclic voltammetry has been used for the optimization of redox behaviour as well as the estimation of specific capacitance. On the other hand, galvanostatic charge-discharge method could vary with different electrode materials and various current densities for the conformations of modified electrode cyclic stability (Up to 5000 cycles). Therefore, the above discussed electrodes, morphological structures, electrochemical techniques and all electrochemical parameters will continue to play an important role in supercapacitor energy storage devices.

#### ACKNOWLEDGEMENT

We gratefully acknowledged, The Management and Chemistry Department Staff members, The Madura College, Madurai, Tamil Nadu, India. And also we thankful to Dr.Pandi Gajendran, Assitant Professor, The Madura College, Madurai and Mr.Abhijit Manna, JRF, SBS, DAB & P, MKU, for their valuable discussion in this article.

#### References

1. O. Bohkn, J. Kowal and D.V. Sauer, *J. Power Sources*, 172 (2007) 468.
2. J.R. Miller, *Electrochim. Acta*, 52 (2006) 1703.
3. Y. Song, S. Hu, D. X. Dong, Y. Wang, C. Wang, C. Wang and Y. Xia, *Electrochim Acta*, 146 (2014) 485.
4. Z. Zhang, C. Zhao, S. Min and X. Qian, *Electrochim. Acta*, 144 (2014) 100.
5. J.Q. Xing, Y.L. Zhou, Q.W. Zhou, X.D. Zheng and Q.J. Jiao, *Electrochim. Acta*, 136 (2014) 550.
6. M. Li, Y. Zhang, L. Yang, Y. Liu and J. Yao, *Electrochim. Acta*, 166 (2015) 310.
7. T.T. Chen, W.L. Song and L.Z. Fan, *Electrochim. Acta*, 165 (2015) 92.
8. G.F. Chen, Z.Q. Liu, J.M. Lin, N. Li and Y.Z. Su, *J. Power Sources*, 283 (2015) 484.
9. B. Fang and L. Binder, *J. Power Sources*, 163 (2006) 616.
10. V. Gupta, S. Gupta and N. Miura, *J. Power Sources*, 177 (2008) 685.

11. W.X. Feng, R.D. Bo and Y. Zheng, *Trans. Nanoferrous. Met. Soc. China*, 16 (2006) 1129.
12. S.J. Bao, C.M. Li, C.X. Guo and Y. Qiao, *J. Power Sources*, 180 (2008) 676.
13. H. Guo and Q. Gao, *J. Power Sources*, 186 (2009) 551.
14. S.W. Hwang and S.H. Hyun, *J. Nonocrystalline Solids*, 347 (2004) 238.
15. Y. Xu, J. Wang, W. Sun and S. Wang, *J. Power Sources*, 159 (2006) 370.
16. B.C. Kim, G.C. Wallace, Y.I. Yoon, J.M. Ko and C.O. Too, *Synth. Met.*, 159 (2009) 1389.
17. A.K.C. Gallegos and M.E. Rincon, *J. Power Sources*, 162 (2006) 743.
18. C. Merino, P. Soto, E.V. Ortego, J.M.G. Salazar, F. Pico and J.M. Rojo, *Carbon*, 43 (2005) 551.
19. R.K. Sharma, H.S. Oh, Y.G. Shul and H. Kim, *J. Power Sources*, 173 (2007) 1024.
20. V.D. Patake and C.D. Lokhande, *Appl. Surf. Sci.*, 254 (2008) 2820.
21. H. Liang, F. Chen, R. Li, L. Wang and Z. Deng, *Electrochim. Acta*, 49 (2004) 3463.
22. K.J. Babu, A. Zahoor, K.S. Nahm, R. Ramachandran, M.A.J. Rajan and G. Gnanakumar, *J. Nanopart. Res.*, 16 (2014) 2250.
23. R. Ramachandran, V. Mani, S.M. Chen, G. Gnanakumar and M. Govindasamy, *Int. J. Electrochem. Sci.*, 10 (2015) 859.
24. R. Ramachandran, V. Mani, S.M. Chen, G. Gnanakumar, P. Gajendran, N.B. Devi and R. Devasenathipathy, *Int. J. Electrochem. Sci.*, 10 (2015) 3301.
25. S.M. Chen, R. Ramachandran, V. Mani and R. Saraswathi, *Int. J. Electrochem. Sci.*, 9 (2014) 4072.
26. V. Mani, R. Devasenathipathy, S.M. Chen, K. Kohilarani and R. Ramachandran, *Int. J. Electrochem. Sci.*, 10 (2015) 1199.
27. S. Ye, J. Feng and P. Wu, *ACS. Appl. Mater. Interfaces*, 5 (2013) 7122.
28. Z. Lei, F. Shi and L. Lu, *ACS. Appl. Mater. Interfaces*, 4 (2012) 1058.
29. T.M. Higgins, D. Mcateer, J.C.M. Coelho, B.M. Sanchez, Z. Gholamvand, G. Moriarty, N. Mcevoy, N.C. Berner, G.S. Duesberg, V. Nicolosi and J.N. Coleman, *ACS Nano*, 8 (2014) 9567.
30. Y. Tan, C. Xu, G. Chen, Z. Liu, M. Ma, Q. Xie, N. Zheng and S. Yao, *ACS. Appl. Mater. Interfaces*, 5 (2013) 2241.
31. H. Sun, W. He, C. Zong and L. Lu, *ACS. Appl. Mater. Interfaces*, 5 (2013) 2261.
32. M. Zhi, F. Yang, F. Meng, M. Li, A. Manivannan and N. Wu, *ACS. Sustainable. Chem. Eng.*, 2 (2014) 1592.
33. M.G. Hahm, A.L.M. Reddy, D.P. Cole, M. Rivera, J.A. Vento, J. Nam, H.Y. Jung, Y.L. Kim, N.T. Narayanan, D.P. Hashim, C. Galande, Y.J. Jung, M. Bundy, S. Karna, P.M. Ajayan and R. Vajtai, *Nano Lett.*, 12 (2012) 5616.
34. X. Zheng, X. Yan, Y. Sun, Z. Bai, G. Zhang, Y. Shen, Q. Liang and Y. Zhang, *ACS. Appl. Mater. Interfaces*, 7 (2015) 2480.
35. Y. Lei, J. Li, Y. Wang, L. Gu, Y. Chang, H. Yuan and D. Xiao, *ACS. Appl. Mater. Interfaces*, 6 (2014) 1773.
36. D. Lan, Y. Chen, P. Chen, X. Chen, X. Wu, X. Pu, Y. Zeng and Z. Zhu, *ACS. Appl. Mater. Interfaces*, 6 (2014) 11839.
37. X.C. Dong, H. Xu, X.W. Wang, Y.X. Huang, M.B.C. Park, H. Zhang, L.H. Wang, W. Huang and P. Chen, *ACS Nano*, 6 (2012) 3206.
38. M. Kim and J. Kim, *ACS. Appl. Mater. Interfaces*, 6 (2014) 9036.
39. M.H. Bai, L.J. Bian, Y. Song and X.X. Liu, *ACS. Appl. Mater. Interfaces*, 6 (2014) 12656.
40. P. Li, Y. Yang, E. Shi, Q. Shen, Y. Shang, S. Wu, J. Wei, K. Wang, H. Zhu, Q. Yuan, A. Cao and D. Wu, *ACS. Appl. Mater. Interfaces*, 6 (2014) 5228.
41. W. Fan, C. Zhang, W.W. Tjiu, K.P. Pramoda, C. He and T. Liu, *ACS. Appl. Mater. Interfaces*, 5 (2013) 3382.
42. Z. Zhou, Y. Zhang, Y. Li and J. Liu, *Nano Lett.*, 13 (2013) 2078.
43. S. Cho, K.H. Shin and J. Jang, *ACS. Appl. Mater. Interfaces*, 5 (2013) 9186.
44. G.M. Suppers, B.A. Deore and M.S. Freund, *Langmuir*, 24 (2008) 1064.

45. C. Bora, J. Sharma and S. Dolui, *J. Phys. Chem. C*, 118 (2014) 29688.
46. D.W. Wang, F. Li, J. Zhao, W. Ren, Z.G. Chen, J. Tun, Z.S. Wu, I. Gentle, G.Q. Lu and H.M. Cheng, *ACS Nano*, 3 (2009) 1745.
47. A.K. Mishra and S. Ramaprabhu, *J. Phys. Chem. C*, 115 (2011) 14006.
48. Y. Jin, H. Chen, M. Chen, N. Liu and Q. Li, *ACS Appl. Mater. Interfaces*, 5 (2013) 3408.
49. L. Deng, R.J. Young, I.A. Kinloch, A.M. Abdelkader, S.M. Holones, D.A.D.H.D. Rio and S.J. Eichhorn, *ACS Appl. Mater. Interfaces*, 5 (2013) 9983.
50. S. Dhibar, P. Bhattacharya, D. Gosh, G. Hatui and C.K. Das, *Ind. Eng. Chem. Res.*, 53 (2014) 13030.
51. S. Dhibar and C.K. Das, *Ind. Eng. Chem. Res.*, 53 (2014) 3495.
52. H. Jiang, Y. Dai, Y. Hu, W. Chen and C. Li, *ACS Sustainable Chem. Eng.*, 2 (2014) 70.
53. H. Chen, S. Zhou and L. Wu, *ACS Appl. Mater. Interfaces*, 6 (2014) 8621.
54. A. Vu, X. Li, J. Philips, A. Han, W.H. Smyrl, P. Buhlmann and A. Stein, *Chem. Mater.*, 25 (2013) 4137.
55. Y. Kumar, G.P. Pandey and S.A. Hashmi, *J. Phys. Chem. C*, 116 (2012) 26118.
56. Y. Lu, K. Fu, S. Zhang, Y. Li, C. Chen, J. Zhu, M. Yanilmaz, M. Dirican and X. Zhang, *J. Power Sources*, 273 (2015) 502.
57. Y. Zhao, M. Liu, L. Gan, X. Ma, D. Zhu, Z. Xu and L. Chen, *Energy Fuels*, 28 (2014) 1561.
58. H. Itoi, H. Nishihara, T. Kogure and T. Kyotani, *J. Am. Chem. Soc.*, 133 (2011) 1165.
59. H. Qiu, T. Bechtold, L. Le and W.Y. Lee, *Power Technology*, 270 (2015) 192.
60. A.L. Zubaidi, T. Inoue, T. Matsushita, Y. Ishii, T. Hashimoto and S. Kawasaki, *J. Phys. Chem. C*, 116 (2012) 7681.
61. Z. Yan, L. Ma, Y. Zhu, I. Lahiri, M.G. Hahm, Z. Liu, S. Yang, C. Xiang, W. Lu, Z. Peng, Z. Sun, C. Kittrel, J. Lou, W. Choi, P.M. Ajayan and J.M. Tour, *ACS Nano*, 7 (2013) 58.
62. H. Konno, T. Kasashima and K. Azumi, *J. Power Sources*, 191 (2009) 623.
63. N. Terasawa and K. Asaka, *Langmuir*, 30 (2014) 14343.
64. R. Satish, V. Aravindan, W.C. Ling and S. Madhavi, *J. Power Sources*, 281 (2015) 310.
65. J. Yin, L. Qi and H. Wang, *ACS Appl. Mater. Interfaces*, 3 (2011) 4315.
66. H. Wang, Z. Xu, Z. Li, K. Cui, J. Ding, A. Kohandehghan, X. Tan, B. Zahiri, B.C. Olsen, C.M.B. Holt and D. Mitlin, *Nano Lett.*, 14 (2014) 1987.
67. M. Chiku, M. Toda, E. Higuchi and H. Inoue, *J. Power Sources*, 286 (2015) 193.
68. X. Xiao, C. Zheng, S. Lin, L. Huang, Z. Hu, Y. Cheng, T. Li, W. Qiao, D. Long, Y. Huang, L. Mai, Y. Gogosti and J. Zhou, *Energy Storage Materials*, 1 (2015) 1.
69. K. Zhuo, M.G. Jeong, M.S. Shin, W.W. Chun, J.W. Bae, P.J. Yoo and C.H. Chung, *Applied Surface Science*, 322 (2014) 15.
70. M. Kundu and L. Liu, *J. Power Sources*, 243 (2013) 676.
71. C.C. Hu, C.M. Huang and K.H. Cheng, *J. Power Sources*, 185 (2008) 1594.
72. V.D. Nithya, B. Hanitha, S. Surendran, D. Kalpana and R. Kalaiselvan, *Ultrason. Sonochem.*, 22 (2015) 300.
73. C.J. Hung, P. Lin and T.Y. Tseng, *J. Power Sources*, 259 (2014) 145.
74. X. Gong, J.P. Cheng, F. Liu, L. Zhang and X. Zhang, *J. Power Sources*, 267 (2014) 610.
75. H.M. Jeong, J.W. Lee, W.H. Shin, Y.J. Choi, H.J. Shin, J.K. Kang and J.W. Choi, *Nano Lett.*, 11 (2011) 2472.
76. X. Han, M.R. Funk, F. Shen, Y.C. Chen, Y. Li, C.J. Campbell, J. Dai, X. Yang, J.W. Kim, Y. Liao, J.W. Connell, V. Barone, Z. Chen, Y. Lin and L. Hu, *ACS Nano*, 8 (2014) 8255.
77. M. Jing, Y. Yang, Y. Zhu, H. Hou, Z. Wu and X. Ji, *Electrochim. Acta*, 141 (2014) 234.
78. C.C. Liu, D.S. Tsai, D. Susanti, W.C. Yeh, Y.S. Huang and F.J. Liu, *Electrochim. Acta*, 55 (2010) 5768.
79. E. Mitchell, F.D. Souza, R.K. Gupta, P.K. Kahol, D. Kumar, L. Dong and B.K. Gupta, *Power Technology*, 272 (2015) 295.

80. P. Staiti, A. Arenillas, F. Lufrano and J.A. Menendez, *J. Power Sources*, 214 (2014) 137.
81. D. Aradilla, M.M.P. Madrigal, F. Estrany, D. Azambuja, J.I. Iribarren and C. Aleman, *Org. Electron.*, 14 (2013) 1483.
82. Q. Zhou, J. Xing, Y. Gao, X. Lv, Y. He, Z. Guo and Y. Li, *ACS. Appl. Mater. Interfaces*, 6 (2014) 11394.
83. S. Nagamuthu, S. Vijayakumar and G. Muralidharan, *Ind. Eng. Chem. Res.*, 52 (2013) 18262.
84. X. Zhang, X. Zeng, M. Yang and Y. Qi, *ACS. Appl. Mater. Interfaces*, 6 (2014) 1125.
85. X. Li, J. Shen, N. Li and M. Ye, *J. Power Sources*, 282 (2015) 194.
86. R.C. Ambare, S.R. Bharadwaraj and B.J. Lokhande, *Appl. Surf. Sci.*, 349 (2015) 887.
87. R. Thangappan, S. Kalaiselvam, A. Elayaperumal and R. Jeyavel, *Solid State Ionics*, 268 (2014) 321.
88. M. Li, W. Guo, H. Li, S. Xu, C. Qu and B. Yang, *Appl. Surf. Sci.*, 317 (2014) 1100.
89. J. Hao, Y. Zhong, Y. Liao, D. Shu, Z. Kang, X. Zou, C. He and S. Guo, *Electrochim. Acta*, 167 (2015) 412.
90. B. You, J. Jiang and S. Fan, *ACS. Appl. Mater. Interfaces*, 6 (2014) 15302.
91. Q. Ji, X. Zhao, H. Liu, L. Guo and J. Qu, *ACS. Appl. Mater. Interfaces*, 6 (2014) 9496.
92. R.B. Rakhi, W. Chen, M.N. Hedhili, D. Cha and H.N. Alshareef, *ACS. Appl. Mater. Interfaces*, 6 (2014) 4196.
93. X. Liu, M. Zhen, Y. Xiao, Y. Yang, L. Yang, Y. Liu, B. Lei, H. Dong, H. Zhang and H. Fu, *ACS. Appl. Mater. Interfaces*, 5 (2013) 4667.
94. K. Wang, Y. Wang, Y. Wang, E. Hosono and H. Zhou, *J. Phys. Chem. C*, 113 (2009) 1093.
95. P. Wang, H. He, X. Xu and Y. Jin, *ACS. Appl. Mater. Interfaces*, 6 (2014) 1563.
96. S. Nagamuthu, S. Vijayakumar and G. Muralidharan, *Energy Fuels*, 27 (2013) 3508.
97. S. Chou, F. Cheng and J. Chen, *J. Power Sources*, 162 (2006) 727.
98. S.K. Meher, P. Justin and G.R. Rao, *ACS. Appl. Mater. Interfaces*, 3 (2011) 2063.
99. S. Wang, C. Han, J. Wang, J. Deng, M. Zhu, J. Yao, H. Li and Y. Wang, *Chem. Mater*, 26 (2014) 6872.
100. X. Meng, M. Zhou, X. Li, J. Yao, F. Liu, H. He, P. Xiao and Y. Zhang, *Electrochim. Acta*, 109 (2013) 20.
101. Y. Lei, J. Li, Y. Wang, L. Gu, Y. Chang, H. Yuan and D. Xiao, *ACS. Appl. Mater. Interfaces*, 6 (2014) 1773.
102. R. Mukkabla, M. Deepa and A.K. Srivastava, *Electrochim. Acta*, 164 (2015) 171.
103. C. Mondal, M. Ganguly, P.K. Manna, S.M. Yusuf and T. Pal, *Langmuir*, 29 (2013) 9179.
104. Y. Tang, Y. Liu, S. Yu, W. Guo, S. Mu, H. Wang, Y. Zhao, L. Hou, Y. Fan and F. Gao, *Electrochim. Acta*, 161 (2015) 279.
105. J. Cai, H. Niu, Z. Li, Y. Du, P. Cizek, Z. Xie and H. Xiong, *ACS. Appl. Mater. Interfaces*, 7 (2015) 14946.
106. B.H. Kim, K.S. Yang and J.P. Ferraris, *Electrochim. Acta*, 75 (2012) 325.
107. L. Yang, S. Chen, Y. Ding, X. Zhou, Z.L. Wang and M. Liu, *Nano Lett.*, 12 (2012) 321.
108. H. Mi, X. Zhang, S. Yang, X. Ye and J. Luo, *Mater. Chem. Phys.*, 112 (2008) 127.
109. C. Tran, R. Sighal, D. Lawrence and V. Kalra, *J. Power Sources*, 293 (2015) 373.
110. Y.H. Hsu, C.C. Lai, C.L. Ho and C.T. Lo, *Electrochim. Acta*, 127 (2014) 369.
111. J.H. Lin, T.H. Ko, Y.H. Lin and C.K. Pan, *Energy Fuels*, 23 (2009) 4668.
112. X. Xia, J. Tu, Y. Zhang, X. Wang, C. Gu, X.B. Zhao and H.J. Fan, *ACS Nano*, 6 (2012) 5531.
113. N. Liu, J. Li, W. Ma, W. Liu, Y. Shi, J. Tao, X. Zhang, J. Su, L. Li and Y. Gao, *ACS. Appl. Mater. Interfaces*, 6 (2014) 13627.
114. J. Xu, K. Wang, S.Z. Zu, B.H. Han and Z. Wei, *ACS Nano*, 4 (2010) 5019.
115. J. Jiang, J. Liu, R. Ding, J. Zhu, Y. Li, A. Hu, X. Li and X. Huang, *ACS. Appl. Mater. Interfaces*, 3 (2011) 99.
116. X. Xia, D. Chao, Z. Fan, C. Guan, X. Cao, H. Zhang and H.J. Fan, *Nano Lett.*, 14 (2014) 1651.

117. K. Zhang, H. Chen, X. Wang, D. Guo, C. Hu, S. Wang, J. Sun and Q. Leng, *J. Power Sources*, 268 (2014) 522.
118. Z.L. Wang, X.J. He, S.H. Ye, Y.X. Tong and G.R. Li, *ACS. Appl. Mater. Interfaces*, 6 (2014) 642.
119. L. Li, A.R.O. Raji, H. Fei, Y. Yang, E.L.G. Samuel and J.M. Tour, *ACS. Appl. Mater. Interfaces*, 5 (2013) 6622.
120. J. Xu, Q. Wang, X. Wang, Q. Xiang, B. Liang, D. Chen and G. Shen, *ACS Nano*, 7 (2013) 5453.
121. C.J. Raj, B.C. Kim, W.J. Cho, S. Park, H.T. Jeong, K. Yoo and K.H. Yu, *J. Electroanal. Chem.*, 747 (2015) 130.
122. S. Vadivel, A.N. Naveen, U.P. Kamalakannan, P. Cao and N. Balasubramanian, *ACS. Appl. Mater. Interfaces*, 351 (2015) 635.
123. G.K. Veerasubramani, K. Krishnamoorthy, R. Sivaprakasam and S.J. Kim, *Mater. Chem. Phys.*, 147 (2014) 836.
124. J. Ji, L.L Zhang, H. Ji, Y. Li, X. Zhao, X. Bai, X. Fan, F. Zhang and R.S. Ruoff, *ACS Nano*, 7 (2013) 6237.
125. K. Deori, S.K. Ujjain, R.K. Sharma and S. Deka, *ACS. Appl. Mater. Interfaces*, 5 (2013) 10665.
126. B. Saravanakumar, K.K. Prushothaman and G. Muralidharan, *ACS. Appl. Mater. Interfaces*, 4 (2012) 4484.
127. D.S. Dhawale, M.R. Benzigar, M.A. Wahab, C. Anand, S. Varghese, V.V. Balasubramanian, S.S. Aldeyab, K. Ariga and A. Vinu, *Electrochim. Acta*, 77 (2012) 256.
128. Z.J. Zhang, L.X. Cheng and X.Y. Chen, *Electrochim. Acta*, 161 (2015) 84.
129. T.E. Rufford, D.H. Jurcakova, Z. Zhu and G.Q. Lu, *Electrochem. Commun.*, 10 (2008) 1594.
130. Y. Yan, E. Khoo, A. Sumboja and P.S. Lee, *ACS Nano*, 4 (2010) 4247.
131. D. Cai, D. Wang, B. Liu, Y. Wang, Y. Li, L. Wang, H. Li, H. Huang, Q. Li and T. Wang, *ACS. Appl. Mater. Interfaces*, 5 (2013) 12905.
132. J.S. Kim, S.S. Shin, H.S. Han, L.S. Oh, D.H. Kim, J.H. Kim, K.S. Hong and J.Y. Kim, *ACS. Appl. Mater. Interfaces*, 6 (2014) 268.
133. S. Cho, K.H. Shin and J. Jang, *ACS. Appl. Mater. Interfaces*, 5 (2013) 9186.
134. X. Zhang, X. Wang, L. Jiang, H. Wu, C. Wu and J. Su, *J. Power Sources*, 216 (2012) 290.
135. V. Sahu, S. Shekhar, R.K. Sharma and G. Singh, *ACS. Appl. Mater. Interfaces*, 7 (2015) 3110.
136. P. Sen, A. De, A.D. Chowdhury, S.K. Bandyopadhyay, N. Agnihotri and M. Mukherjee, *Electrochim. Acta*, 108 (2013) 265.
137. Y. Yao, C. Ma, J. Wang, W. Qiao, L. Ling and D. Long, *ACS. Appl. Mater. Interfaces*, 7 (2015) 4817.
138. X. Liu, L. Zhou, Y. Zhao, L. Bian, X. Feng and Q. Pu, *ACS. Appl. Mater. Interfaces*, 5 (2013) 10280.
139. G. Yu, L. Hu, N. Liu, H. Wang, M. Vosgueritchian, Y. Yang, Y. Cui and Z. Bao, *Nano Lett.*, 11 (2011) 4438.
140. S. Saha, M. Jana, P. Khanra, P. Samanta, H. Koo, N.C. Murmu and T. Kuila, *ACS. Appl. Mater. Interfaces*, 7 (2015) 14211.
141. B. Anothumakkool, A. Torris, S.N. Bhange, S.M. Unni, M.V. Badiger and S. Kurungot, *ACS. Appl. Mater. Interfaces*, 5 (2013) 13397.
142. Y. He, W. Chen, X. Li, Z. Zheng, J. Fu, C. Zhao and E. Xie, *ACS Nano*, 7 (2013) 174.
143. X. Li, L. Yang, Y. Lei, L. Gu and D. Xiao, *ACS. Appl. Mater. Interfaces*, 6 (2014) 19978.
144. J. Han, L.L. Zhang, S. Lee, J. Oh, K.S. Lee, J.R. Potts, J. Ji, X. Zhao, R.S. Ruoff and S. Park, *ACS Nano*, 7 (2013) 19.
145. L. Bao, J. Zhang and X. Li, *Nano Lett.*, 11 (2011) 1215.
146. D. Cai, H. Huang, D. Wang, B. Liu, L. Wang, Y. Liu, Q. Li and T. Wang, *ACS. Appl. Mater. Interfaces*, 6 (2014) 15905.
147. J. Zhang and J.W. Lee, *ACS Sustainable Chem. Eng.*, 2 (2014) 735.

148. D. Ghosh, S. Giri and C.K. Das, *ACS Sustainable Chem. Eng.*, 1 (2013) 1135.
149. M. Kotal, A.K. Thakur and A.K. Bhowmick, *ACS. Appl. Mater. Interfaces*, 5 (2013) 8374.
150. C.Y. Hsu, H.W. Chen, K.M. Lee, C.W. Hu and K.C. Ho, *J. Power Sources*, 195 (2010) 6232.
151. Z.Y. Sui, Y.N. Meng, P.W. Xiao, Z.Q. Zhao, Z.X. Wei and B.H. Han, *ACS. Appl. Mater. Interfaces*, 7 (2015) 1431.
152. C. Feng, J. Zhang, Y. He, C. Zhong, W. Hu, L. Liu and Y. Deng, *ACS Nano*, 9 (2015) 1730.
153. Z. Xu, Z. Li, C.M.B. Holt, X. Tan, H. Wang, B.S. Amirkhiz, T. Stephenson and D. Mitlin, *J. Phy. Chem. Lett.*, 3 (2012) 2928.
154. H. Gao, F. Xio, C.B. Ching and H. Duan, *ACS. Appl. Mater. Interfaces*, 4 (2012) 2801.
155. Z. Peng, J. Lin, R. Ye, E.LG. Samuel and J.M. Tour, *ACS. Appl. Mater. Interfaces*, 7 (2015) 3414.
156. Y. Lim, J. Yoon, J. Yun, D. Kim, S.Y. Hong, S.J. Lee, G. Zi and J.S. Ha, *ACS Nano*, 8 (2014) 11639.
157. W.J. Cao, M. Greenleaf, Y.X. Li, D. Adams, M. Hagen, T. Doung and J.P. Zheng, *J. Power Sources*, 280 (2015) 600.
158. T. Tevi, H. Yaghoubi, J. Wang and A. Takshi, *J. Power Sources*, 241 (2013) 589.
159. M. Chen, H. Wang, L. Li, Z. Zhang, C. Wang, Y. Liu, W. Wang and J. Gao, *ACS. Appl. Mater. Interfaces*, 6 (2014) 14327.
160. Y. Pan, F. Zeng, Z. Huang, H. Zhou and Y. Kuang, *Electrochim. Acta*, 172 (2015) 71.
161. G. Luo, L. Liu, J. Zhang, G. Li, B. Wang and J. Zhao, *ACS. Appl. Mater. Interfaces*, 5 (2013) 11184.
162. Y. Yin, C. Liu and S. Fan, *J. Phys. Chem. C*, 116 (2012) 26185.
163. C.T. Hsu, C.C. Hu, T.H. Wu, J.C. Chen and M. Rajkumar, *Electrochim. Acta*, 146 (2014) 759.
164. C. Wang, Y. Zhou, L. Sun, Q. Zhao, X. Zhang, P. Wan and J. Qiu, *J. Phys. Chem. C*, 117 (2013) 14912.
165. J. Zhu, W. Shi, N. Xiao, X. Rui, H. Tan, X. Lu, H.H. Hng, J. Ma and Q. Yan, *ACS. Appl. Mater. Interfaces*, 4 (2012) 2769.
166. S. Zhou, J. Xu, Y. Xiao, N. Zhao and C.P. Wong, *Nano Energy*, 13 (2015) 458.
167. C. Fang, J. Zhang, Y. Deng, C. Zhong, L. Liu and W. Hu, *Mater. Sci. Eng., B*, 199 (2015) 15.
168. W. Singsang, M. Panapoy and B. Ksapabutr, *Energy Procedia*, 56 (2014) 439.
169. Z. Ma, X. Huang, S. Dou, J. Wu and S. Wang, *J. Phys. Chem. C*, 118 (2014) 17231.
170. P. Yu, Y. Li, X. Zhao, L. Wu and Q. Zhang, *Langmuir*, 30 (2014) 5306.
171. X. Liu, S. Shi, Q. Xiong, L. Li, Y. Zhang, H. Tang, C. Gu, X. Wang and J. Tu, *ACS. Appl. Mater. Interfaces*, 5 (2013) 8790.
172. W. Zhang, B. Quan, C. Lee, S.K. Park, X. Li, E. Choi, G. Diao and Y. Piao, *ACS. Appl. Mater. Interfaces*, 7 (2015) 2404.
173. F.K. Butt, M. Tahir, C. Cao, F. Idrees, R. Ahmed, W.S. Khan, Z. Ali, N. Mohmood, M. Tanveer, A. Mohmood and I. Aslam, *ACS. Appl. Mater. Interfaces*, 6 (2014) 13635.
174. C.H. Wu, S. Deng, H. Wang, Y. Sun, J. Liu and H. Yan, *ACS. Appl. Mater. Interfaces*, 6 (2014) 1106.